高圧下で合成された充填スクッテルダイト化合物 Smy(Fe1-xNix)4Sb12 の熱電特性

DISSERTATION

THERMOELECTRIC PROPERTIES OF FILLED SKUTTERUDITE COMPOUNDS $Sm_y(Fe_{1-x}Ni_x)_4Sb_{12}$ PREPARED UNDER HIGH PRESSURE

MURORAN INSTITUTE OF TECHNOLOGY

Doctor of Engineering

Course of Advanced Information and Electronic Engineering

Physics of Strongly Correlated Electron Systems Laboratory

Admission in 2017

Student ID number 17096506

ATCHARIYA PHUANGYOD

Submission in 2020

THERMOELECTRIC PROPERTIES OF FILLED SKUTTERUDITE COMPOUNDS $Sm_y(Fe_{1-x}Ni_x)_4Sb_{12}$ PREPARED UNDER HIGH PRESSURE

by

Atchariya Phuangyod

A dissertation submitted in partial fulfillment of the requirements for the degree of Doctor of Engineering

Examination Committee:	Prof. Sekine Chihiro
Nationality:	Thai
Previous Degree:	Bachelor of Electrical Engineering Chiang Mai University, Thailand Master of Energy Engineering Chiang Mai University, Thailand
Scholarship Donor:	Japan Student Services Organization (JASSO) Muroran Institute of technology (MuIT) Scholarship

Muroran Institute of Technology
Japan

September 2020

ACKNOWLEGEMENT

The author wishes to express her profound gratitude to her advisor, Prof. Sekine Chihiro for her supporting study, helping with living in a foreign country, friendly discussions, helps to reduce study stress, and all valuable efforts for the accomplishment of her study. She thanks also go to Assoc. Prof. Kawamura Yukihiro, Dr. Junichi Hayashi, and her laboratory members for kindly teach her the experiment, and supporting study.

The sincere thanks also go to express her master's graduate advisor, Asst.Prof. Wongkot Wongsapai, and Assoc.Prof. Chatchawan Chaichana, Chiang Mai University, Thailand for encouragement and advice.

The author wishes to special thanks to her beloved family, Ms. Sirirat Phuangyod, Mr. Samrite Phuangyod, Mr. Kha Kuppheng, and Miss Sujitra Kuppheng for the support and encouragement of the author always, and friends whom the author cannot mention name all for making laughter, creating fun, helps relieve stress, always support the author.

Lastly, sincerely thank you to the Muroran Institute of Technology for providing the opportunity to study and to provide the author with a worthwhile experience that is nowhere else.

This study is intended for the self-development of the author. Giving the author the knowledge, ability, and living with others, patience, diligence. The author is extremely ecstatic, and very grateful to these precious experiences.

Topic: Thermoelectric properties of filled skutterudite compounds $Sm_y(Fe_{1-x}Ni_x)_4Sb_{12}$ prepared under high-pressure

Author: Atchariya Phuangyod

Degree: Doctor of Engineering

Course: Advanced Information and Electronic Engineering

Advisor: Professor Sekine Chihiro

ABSTRACT

Filled skutterudite compounds are one type of TE that suitable for the use of advanced TE potentials of applications. It has been studied as one of the most promising TE based on Phonon Glass Electron Crystal (PGEC) concept implying, these have a phonon of crystal that is "glass-like" behavior, lattice thermal conductivity like amorphous material but an electronic structure like solid crystalline.

In this study, thermoelectric properties of p-type and n-type filled skutterudites $Sm_y(Fe_{1-x}Ni_x)_4Sb_{12}$ samples as the nominal composition of $0 \leq Ni \leq 0.56$ and $0.1 \leq Sm \leq 1.2$ prepared by the high-pressure technique at pressure up to 2 GPa. The samples were characterized by X-ray diffraction (XRD). The actual element was estimated by a scanning electron microscopy (SEM) with an energy-dispersive X-ray spectrometry (EDX), and the electron probe microanalyzer (EPMA), respectively. The electrical resistivity was estimated by the Cryostat vacuum system with a standard dc four-probe method, the thermal conductivity, the Seebeck coefficient measurements, and Hall effect were performed by a physical property measurement system (Quantum Design PPMS option TTO) at temperature range 2 K to 300 K. The Seebeck coefficient of samples exhibited the p-type and n-type skutterudite depended on tuning Sm-filled, and Fe/Ni content. The highest *ZT* value of 0.167(7) is achieved for $Sm_{0.09}(Fe_{0.61}Ni_{0.39})_4Sb_{12.5}$ at room temperature.

CONTENTS

LIST OF FIGURES

LIST OF TABLES

LIST OF ABBREVIATIONS

Abbreviation	Definition
AC	Alternating current
DC	Direct current
EDS	Energy dispersive X-ray spectrometer
EDX	Energy dispersive X-ray spectrometry
EPMA	Electron probe microanalyzer
GHGs	Greenhouse gases
HP	Synthesized sample series
HPHT	High-voltage high-temperature technique
HPS	High-pressure synthesis
PFs	Power factor
PGEC	Phonon Glass Electron Crystal
PPMS	The Physical Property Measurement System
RF	Radio Frequency
S	The Seebeck coefficient
SEM	Scanning electron microscopy
ST	Sintered sample series
TE	Thermoelectric
TECs	Thermoelectric coolers
TEGs	Thermoelectric generators
TEM	Thermoelectric modules
TTO	The Quantum Design Thermal Transport option
WDS	A wavelength dispersive X-ray analyzer
XRD	Powder X-ray diffraction
ZT	The dimensionless figure of merit

Chapter 1 Introduction

1.1 Introduction

Global warming caused by global temperature rise. Whether on the air, on the Earth's surface, or in the sea, climate change is a result of human life activities that increase of greenhouse gases (GHGs) in the atmosphere until the greenhouse effect due to the use of natural gas, fuel, and coal to generate electricity. It will become dangerous to humans due to the negative impact on air pollution and global warming that we face in the past 100 years, with an average global temperature rising to 0.18 ^{0}C and from the weather forecasting model 20 years ago, the average global temperature will rise to 1.1 to 6.4 ^{0}C. (1)

Currently, there is a growing interest in the use of renewable energy. To harvest natural energy from the environment to provide sustainable, green, and inexpensive electrical energy such as heat radiation, solar energy, vibration/ mechanical energy, and etc., as well as convert heat into electrical energy to produce electronic devices and industrial machinery is expanding exponentially.(2) Heat energy is one of the energy sources from many places. They can be found in many sectors such as in electronic operations, devices (integrated circuits, telephones, computers, etc.) manufactories, vehicles, in the building sector, and even in the human body.

The principle of thermoelectric (TE) was discovered in 1823 by German scientist Thomas Seebeck, electricity flows continuously if there is a closed circuit of the two different conductors formed and their joints kept at a hot and cold junction. The Peltier effect by Jean Charles Athanase Peltier, Peltier uses electricity as the interface between different conductors of metal in the results of the heat absorption circuit at one joint and the heat released at the other joints as shown in Figure 1.1.1., thermal energy transfer from p- to n-type semiconductor

materials. The thermoelectric converter is a heat engine and, like all types of heater engines, from thermodynamics rules. If we consider a converter that works as an ideal generator without heat loss efficiency is defined as the ratio of electrical energy delivered to the load to the heat absorbed at the hot junction. The creation of a thermoelectric unit is easy to find by considering the simplest origin, consisting of a single thermocouple with a p-type and n-type semiconductor.

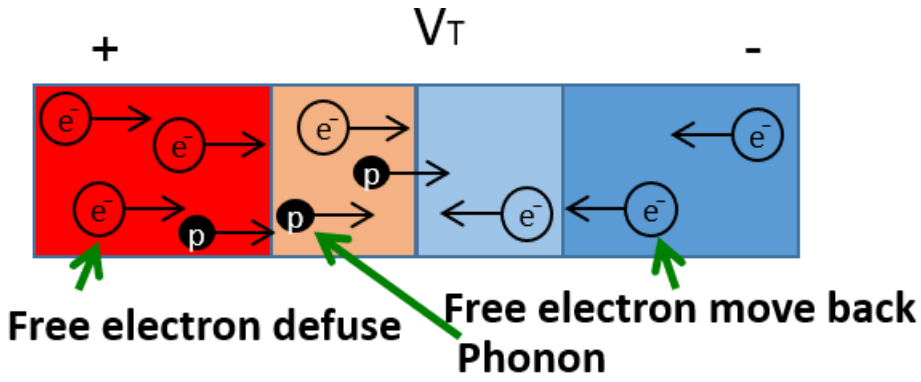

Figure 1.1.1. Thermal energy transfer from p-type to n-type semiconductor materials.

Thermoelectric modules (TEM) are created by the two most popular semiconductor materials, the most commonly used are Bismuth Telluride (Bi_2Te_3). They must have an electron density. different p-type and n-type, connected in parallel circuits and separated between each other by insulating sheets. The semiconductors of p- and n-types are connected by copper strips for electric current flow. The input is provided at the free end of the two semiconductors, temperature differences occur at the semiconductor junctions.

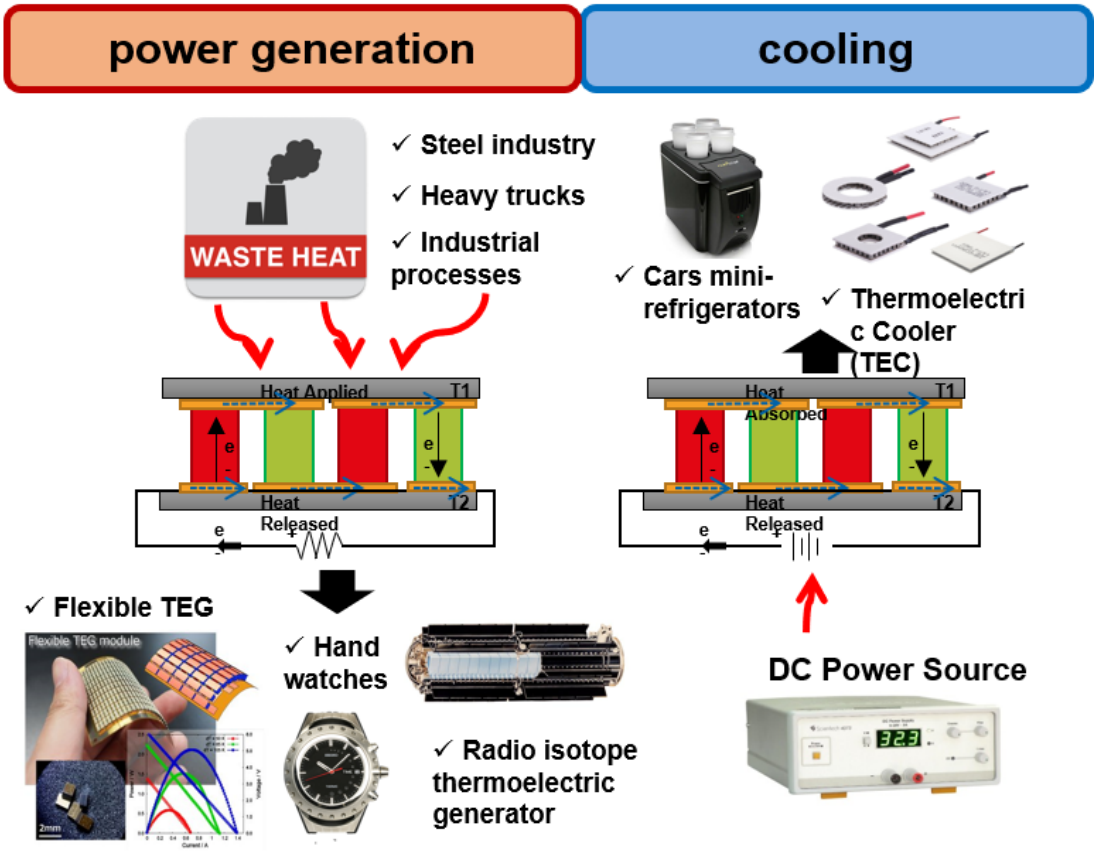

Figure 1.1.2. Thermoelectric modules (TEM) and applications.

Figure 1.1.2. shows thermoelectric modules (TEM) and applications, the power principle can be generated by separating two conductors at hot and cold spots by the Seebeck effect. On the other hand, the reverse of the Seebeck effect is called the Peltier effect, and the Peltier effect creates heating or cooling.(3) TE's diverse energy applications are divided into 2 major groups: 1. power generation, based on the ability to convert temperature differences directly into electrical energy without moving, which waste heat can be converted into electrical energy that are useful in cars such as Thermoelectric generators (TEGs) (2), charging phone system, hand watched, radio isotope thermoelectric generator, and etc., and 2. cooling system, the ability to convert DC electrical energy into cooling such as thermoelectric coolers (TECs), car mini refrigerators and air conditioning systems, small scale cooling system, medical cooler, and etc.

TE is widely used in many fields due to its interesting features such as energy-saving, free maintenance, a long-life span, a high energy density, there are no moving parts, its work is quiet and strong, and etc. The major advantage is that it is not necessary to use toxic refrigerants that are harmful to the environment, but TE main weakness is due to low energy conversion efficiency (4), they become interesting in of energy harvesting for large and small applications, depending on the size of the power output and the materials used.

1.2 Motivation

Filled skutterudite compounds are one type of TE that suitable for the use of advanced TE potentials of applications. It has been studied as one of the most promising TE based on state-of-the-art TE materials possess the feature of Phonon Glass Electron Crystal (PGEC) concept (5),(6),(7) implying, these have a phonon of crystal that is "glass-like" behavior, lattice thermal conductivity like amorphous material but an electronic structure like solid crystalline. The formula was RT_4X_{12}, where R is guest atom such as alkali metal, alkaline earth, lanthanide, and actinide, T is transition metals such as Fe, Ru, Os, Pt, and X is non-metals such as P, As, Sb, Ge, respectively. The random motion (rattling)(5) of R inside the X_{12} voids to scatter the phonon in the crystal structure, which responsible for a substantial decrease in κ_L to affects the electrical transport properties and enhance the Figure of merit ZT values. The devaluation efforts of κ_L could cause a decrease of κ without reducing PFs, aggregated excellent TE will result in high ZT values by high S combined with high σ and low κ values.

The p-type skutterudites originated from the binary compound $CoSb_3$ and shown high-performance ZT value. The partial or total substitution of Co with other transition metals such as Fe and Ni provided that the electron count rule. The successful synthesis of many R-filled $R_y(Fe_{1-x}Ni_x)_4Sb_{12}$ skutterudite compounds, the p-type and the n-type skutterudite has been reported Sm fillers

atoms get the attention of donating electrons to the crystals had improved *PFs* and κ_L value by rattling effect.

These substances have never been prepared by using high-pressure synthesis (HPS) technique before, which this method helps to usually take a few hours, estimated a decrease in synthetic temperature and the densification rate can be improved by a pressure. The potential *ZT* should be achieved by carefully expanding the areas of synthesis with the tune the Sm filling ratio, also the Fe/Ni substitution around the p/n crossover area is attributed to the increase of *S* values. The TE properties can be tuned by the Sm-filled and the substitution Fe/Ni content, the p/n crossover of $Sm_y(Fe_{1-x}Ni_x)_4Sb_{12}$ at Fe ≈ 0.63, and Sm ≈ 0.31 confirmed by measurements of *S* values prepared by direct reaction of the elements at room-temperature, also at Fe ≈ 0.60, and Sm ≈ 0.33 confirmed by measurements of *S* values prepared by spark plasma sintering (SPS). (8)

In this study, investigated the TE properties of p-type and n-type filled skutterudites $Sm_y(Fe_{1-x}Ni_x)_4Sb_{12}$ prepared by HPS technique, It was expected successfully in synthesized under high pressure using multi-anvil press made it possible to enlarge the variation of TE material design. The optimized *ZT* could be achieved by carefully expanding the research areas of synthesis with tuning the Sm filling ratio and the Fe/Ni substitution ratio in the vicinity of the p/n crossover point where high S values were observed.

1.3 References

1. Oakes T. Asia. International Encyclopedia of Human Geography. 2009. 214–219.

2. Jaziri N, Boughamoura A, Müller J, Mezghani B, Tounsi F, Ismail M. A comprehensive review of Thermoelectric Generators: Technologies and common applications. Energy Reports. 2019.

3. Patidar S. Applications of Thermoelectric Energy: A Review. Int J Res Appl Sci Eng Technol. 2018;6(5):1992–6.

4. Kang C, Wang H, Bahk JH, Kim H, Kim W. Thermoelectric materials and devices. Vols. 2015-Janua, RSC Nanoscience and Nanotechnology. 2015;107–141.

5. Rowe EDM, Ph D, Sc D, Group F. HANDBOOK. 2006. 72-82.

6. Srinivasan B. Novel chalcogenide-based glasses, ceramics and polycrystalline materials for thermoelectric application. 2019.

7. Nolas GS, Morelli DT, Tritt TM. Skutterudites: a phonon-glass-electron crystal approach to advanced thermoelectric energy conversion applications. Annu Rev Mater Sci. 1999; 29:89–116.

8. Artini C, Castellero A, Baricco M, Buscaglia M T and Carlini R, J. Solid State Sci. 2018;79:71-78.

Chapter 2 Theories and literature reviews

2.1 Thermoelectric effect

As is known that equipment is used Widely Thermoelectric (TE) Both temperature measurement of heating or cooling of solids and direct energy conversion from waste heat. Based on the principle of temperature differences, the charged carriers in the material will spread to the hot side to the cold side.(1) The carrier will be moved to the cold side and discarded. Behind the opposite charged nucleus on the hot side, causing a voltage.

The thermoelectric phenomenon allows the conversion of heat into electricity or electricity. The phenomenon is described by three related mechanisms: Seebeck, Peltier, and Thomson effects.(2)

The Seebeck phenomenon is an important phenomenon associated with thermocouples. They are caused by bringing two types of metal conductors connecting the ends together and heating at one connection point, causing electric current to flow in the circuit, the value of electric current changes according to the temperature difference at both ends of the junction as an open circuit. There will be a voltage generated called “Seebeck voltage”.

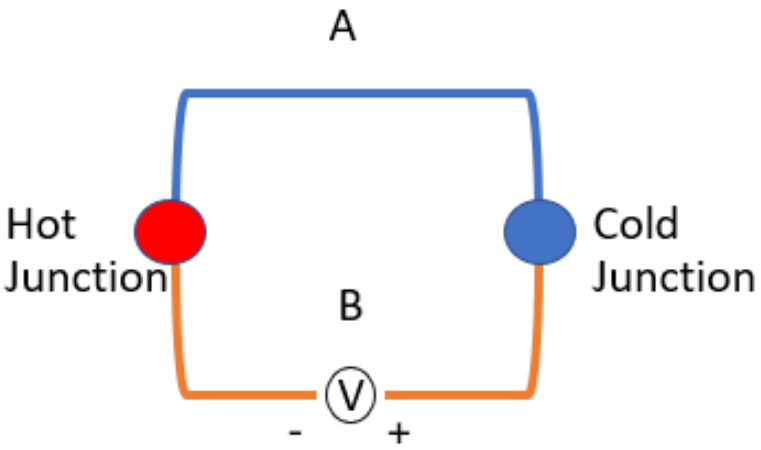

Figure 2.1.1. The Seebeck effect

The seebeck effect as a Figure. 2.1.1, the hot and cold junctions are maintained at different temperatures T_1 and T_2 and $T_1 > T_2$ an open circuit electromotive force (emf), V is developed, and given by

$$V = \alpha (T_1 - T_2) \quad (1)$$

$$\alpha = V/\triangle T \quad (2)$$

, where α is the differential Seebeck coefficient between A and B. The sign of α is positive if the emf causes a current to flow in a clockwise direction around the circuit and is measured in *V/K*.

For the Peltier phenomenon, the reverse phenomenon of the Seebeck phenomenon is that the input of electricity into the circuit will produce one-sided heat. Or the temperature rises to one end of junctions, the other end of junctions is cold or the temperature drops. Causing the direction of the electric current to be inverted. That is, the temperature on both sides is reversed, with the hot side changing to cold or the low temperature.

Thomson's results are related to the reverse heat generation rate q, which is the result of current flows along one part of a single conductor with different temperatures $\triangle T$ as shown in the equation below,

$$q = \beta I \triangle T \tag{3}$$

, where β is Thomson coefficient (V/K). The sign of α is positive if the emf causes a current to flow in a clockwise direction around the circuit and is measured in V/K, by considering this value as well.

2.2 Thermoelectric performance

The material potential for thermoelectric applications (conversion of heat into electricity) is determined by the dimensionless figure of merit (ZT) is a function of carrier concentration, electrical conductivity increases as the carrier concentration increases as shown in the equation below,

$$ZT = \frac{S^2 T}{\rho \kappa} = \frac{S^2 \sigma T}{\kappa_e + \kappa_l} \quad [K^{-1}] \tag{4}$$

$$\kappa = \kappa_e + \kappa_l \tag{5}$$

, where S is the Seebeck coefficient (V/K), T is the absolute temperature (K), ρ is the electrical resistivity (Ω·m), σ is the electrical conductivity (S/m), κ is the total thermal conductivity (W/mK), κ_e is electronic thermal conductivity, and κ_l is Lattice thermal conductivity. The electrical power factor control by $S^2\sigma$ and ZT reflects the efficiency of a thermoelectric solid.

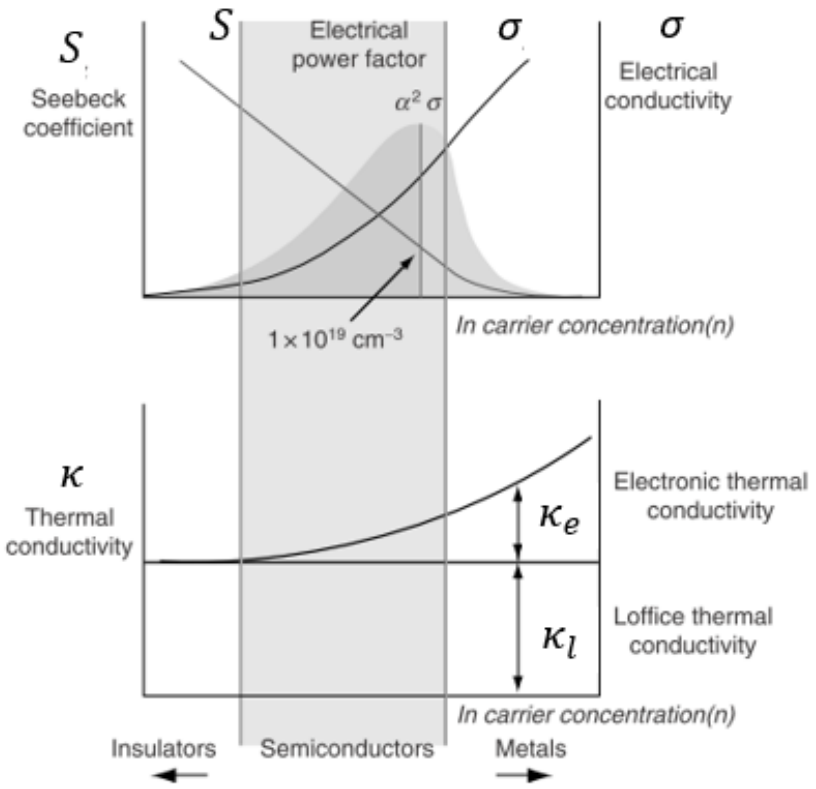

Figure 2.2.1. The electrical conductivity, Seebeck coefficient, power factor, and thermal conductivity depend on carrier concentration.(1)

The classification of materials by electrical conductivity is divided into 3 categories, high electrical conductivity is metal materials. While the low conductivity is insulating material. The conductivity in the middle between the two materials is a semiconductor.

Electrical conductivity is the result of the carrier concentration and all three parameters that occur in the Figure-of-merit as shown in Figure 1.2.1, the electrical conductivity, Seebeck coefficient, power factor, and thermal conductivity depending on the carrier concentration. The Seebeck coefficient decreases with the electrical power factor maximizing at a carrier concentration of around 10^{25}/cm.(1) Generally, in thermoelectric materials is 1/3 of the total thermal conduction increases with the carrier concentration.

ZT value corresponds to the semiconductor material. Therefore, semiconductors are the most researched materials for thermoelectric applications. *ZT* varies with the measurement temperature (*T*). *ZT* > 0.5 (1) are often considered thermoelectric materials.

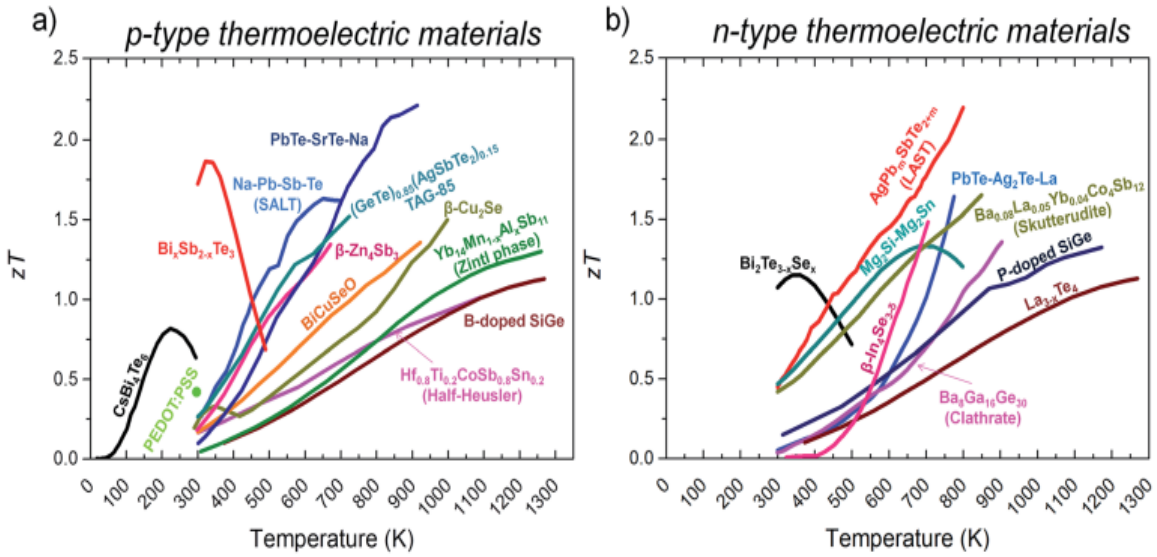

Figure 2.2.2. Performance of p- and n-type thermoelectric materials.

At high temperatures (> 900 K), major improvements have been made to more than one. Figure 2.2.2. shows performance of p- and n-type thermoelectric materials, Si – Ge alloys, $La_{3-x}Te_4$, Zintl phases, phonon-liquid electron-crystal (PLEC), low thermal conductivities due to the high mobility of the copper with superionic behavior, and oxides. It is good performance and environmental friendliness. For telluride or related families presented the best *ZT* known until now for bulk thermoelectric materials, with values of 2.2 at 915 K for p-type PbTe doped with 4% SrTe and 2% Na, 1.6 at 775 K for the n-type doped with Ag_2Te and La, 2.2 at 800 K for $AgPb_{18}SbTe_{20}$ (LAST) n-type compound at 400-800 K (medium temperature range).(3)

It can be concluded that the thermoelectric advances try to focus on the improvement of *ZT* by reducing the thermal conductivity, followed by "PGEC" concept.(1),(4) It proposed that the crystal structure with atoms or molecules with

a gentle "rattling" bond within the atomic cage should conduct heat such as glass. But the electrically conductive materials such as crystals, by the material skutterudites and clathrate, have received attention due to the coherence of this principle.

2.2.1 Thermoelectric parameters

Efficiency of the generator is a function of the ratio of the load resistance to the sum of the resistance generator arms, and at the maximum output power as shown in the equation below,

$$\varphi_p = \frac{T_H - T_C}{\frac{3T_H}{2} + \frac{T_C}{2} + \frac{4}{Z_C}} 1 \tag{6}$$

, where T_H is hot temperature, T_C is cold temperature, Z_c is the Figure-of-merit of the couple ($S^2/\rho\kappa'$), where κ' is the thermal conductance of 2 junction material in parallel and ρ is the series resistance, while the maximum conversion efficiency,

$$\varphi_{max.} = \frac{T_H - T_C}{T_H}\gamma \tag{7}$$

$$\gamma = \frac{\sqrt{1+Z_cT}-1}{\sqrt{1+Z_cT}+\frac{T_C}{T_H}} \tag{8}$$

$$T = \frac{T_H - T_C}{2} \tag{9}$$

And the maximum efficiency is the product of the Carnot efficiency, which is clearly less than unity, and γ, which embodies the parameters of the materials. If the shapes of 2 materials (mat.1, and mat.2, respectively) match up to minimize heat absorption,

$$Z_c = \frac{S^2}{[\left(\frac{\kappa_{\mathrm{mat.1}}}{\sigma_{\mathrm{mat.1}}}\right)^{\frac{1}{2}} + \left(\frac{\kappa_{\mathrm{mat.2}}}{\sigma_{\mathrm{mat.2}}}\right)^{\frac{1}{2}}]^2} \tag{10}$$

Then, figure-of-merit (Z) determines the maximum conversion efficiency at the operating temperature, consists of three transport parameters for a material as shown in the equation below,

$$Z = \frac{S^2\sigma}{\kappa} \tag{11}$$

, where S is the Seebeck coefficient (V/K), σ is the electrical conductivity (S/m), the electrical power factor control by $S^2\sigma$, and κ is the total thermal conductivity (W/mK).

Or we know as the dimensional Figure of merit (ZT), $ZT = \frac{S^2\sigma}{\kappa}T$. The material will have a high ZT value if it has a large Seebeck coefficient, small electrical resistance, and small thermal conductivity. In thermoelectric semiconductor materials total thermal conductivity is an electronic thermal conductivity (κ_e) and lattice thermal conductivity (κ_l), $\kappa = \kappa_e + \kappa_l$

These three transport parameters perform depending on the carrier's concentration, the amendment to one parameter will also affect the other parameters, according to the law of Wiedemann-Franz law, electronic thermal conductivity as shown in the equation below,

$$\kappa_e = \frac{L_0 T}{\rho} \tag{13}$$

$$L_0 = \frac{\pi^2}{3}.\left(\frac{\kappa_B}{e}\right)^2 \tag{14}$$

, where L_0 is the Lorenz number, κ_B is Boltzmann's constant, e is the electronic charge (1.6×10^{-19} C).

In conclusion, the electrical conductivity increases (σ), when the electronic thermal conductivity (κ_e) increase, but no Z value increases. Therefore, the thermoelectric material, which depends on reducing the thermal conductivity (κ) without reducing the power factor by trying to reduce the lattice thermal conductivity (κ_l).

2.2.2 Transport parameters

The Seebeck coefficient (S) and electrical conductivity (σ) depend on the fermi level (η^*), which will depend on the carrier concentration (n), carrier effective mass (m^*), and the temperature. Showing thermoelectric transportation coefficient in the form of fermi energy. The thermal conductivity (κ) depends on the carrier concentration, increase in the carrier concentration effect to increase ZT value providers appears in the form of power factors ($S^2\sigma$) as shown in the equation below,

$$S = \pm\frac{\kappa_B}{e}(2.5 + s - \eta^*) \tag{15}$$

$$\eta^* = \frac{\eta}{\kappa_B T} \tag{16}$$

, where κ_B is Boltzmann's constant, s is the scattering parameter, $\pm$ sign is for valence and conduction band, respectively. In heavy-doped, Seebeck coefficient as shown in the equation below,

$$S = \pm\frac{\kappa_B}{e}\left(\frac{(2+s)F_{1+s}(\eta^*)}{(1+s)F_s(\eta^*)} - \eta^*\right) \tag{17}$$

$$F_n = \int_0^\infty \frac{x^n}{1+\exp\,(x-\eta^*)}\,dx \tag{18}$$

, where F_n is a Fermi integral of the order x, F_s is the exponent of the carrier's energy dependency means the free path. The distribution of the phononic or lattice vibrations of the capacitors (s=0), while the carriers are disrupted from charged impurities (s=2), and the mixed scattering (s=1). The transport electric provider is represented by two mechanisms, the acoustic photons and ionized impurities scattering dependence on the temperature of the carrier concentration (n) were $T^{-3/2}$, $T^{1/2}$(1), respectively.

The material is a single-band semiconductor that non-degenerate, the Seebeck coefficient efficiency as shown in the equation below,

$$S = \pm\frac{\kappa_B}{e}(\eta^* + In\frac{N}{n}) \quad (19)$$

, where N is the density of state, For the material is a single-band semiconductor that degenerate, the Seebeck coefficient efficiency as shown in the equation below,

$$S = \pm\frac{{\kappa_B}^2 T}{eh^2}.m^*.\frac{8\pi^{4/3}}{9n} \quad (20)\sigma$$

, where h is the Planck constant (6.63×10^{-34} Js), and m^* is the carrier effective mass, respectively.

2.2.3 Hall Coefficient, Carrier and Mobility concentration

In the year 1879, student Edwin Hall of the University of John Hoppin found that the production of voltage (Hall voltage) across from one side of the conductor to the other side.(5) This voltage occurs when the magnetic field is perpendicular to the surface of the conductor and the DC voltage is fed to that conductor. The magnetic force forces the electric current from the DC voltage to flow along the edge of the conductor.

The Hall coefficient is defined as the ratio of the induced electric field to the product of the current density and the magnetic field inserted. It is a characteristic of the material that made the conductor Because its value depends on the type, amount, and property of the charge carriers that make up the electric current.

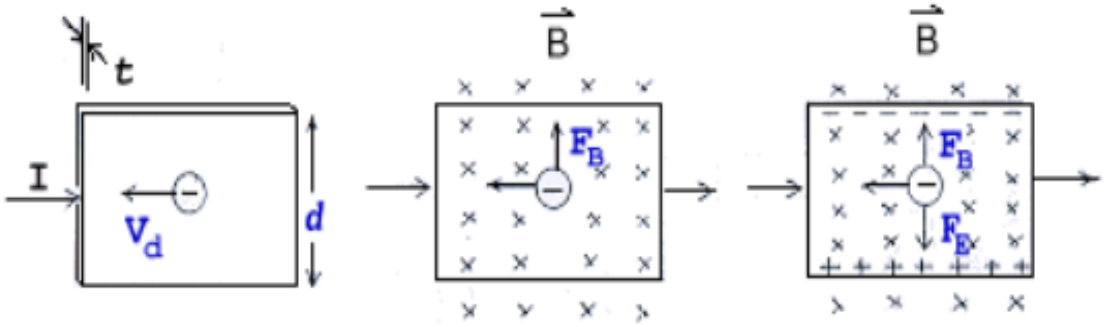

Figure 2.2.3. The occurrence of the hall effect.

Figure 2.2.3 shows a thin conductor sheet with width, thickness and conventional current (I) passes in the direction from the left to the right. The charge carrier is a moving electron (velocity, V_d) in the opposite direction to the current from the right to the left, while the magnetic field (B) is directed towards and perpendicular to the plane of a thin conductor will be the magnetic force (F_B) acting on the electrons causing the electrons to deflect towards the top edge of the thin conductor. Over time, many electrons will be pushed to the top edge. As for the bottom border a large amount of positive charges having different charges on both edges causing an electric field called the Hall field (E_H) in a thin conductor having direction from the bottom edge to the top edge.

The electric field causes the electric force (F_E) acting on the electron, which will cause the electrons to be pushed to the bottom edge. When the electric force and the magnetic force are the same size, the electrons move in the left direction without deflecting, electric field generated in some conductors.

In general, the energy factors of TE materials are adjusted to suit the carrier concentration (n) by measuring Hall effect.(1)

$$V_H = \frac{BIb}{neA} = \frac{R_H BI}{t} \tag{21}$$

$$R_H = \frac{1}{ne} \tag{22}$$

, where V_H is the Hall voltage (V), R_H is the Hall coefficient (cm^3/C), B is a magnetic field (Oe), b is the width of the sample and t is the thickness, and I is conventional current. The electrical conductivity is related to the carrier concentration as show,

$$\sigma = n.e.\mu = 1/\rho \tag{23}$$

, where e is the elementary charge (1.6×10^{-19} C), μ is the carrier mobility are important for fully characterizing and understanding a TE material. An error in the alignment of the conductor (IR voltage) or the magnetic stripe in a straight line may cause an error. This uses a balanced three-wire hall conductor with a magnetic center bridge to eliminate any resistance. There are also other error corrections such as the TE limit, eliminating temperature gradient, other restrictions. Such as van der Pauw limitations, magneto-TE characteristics, etc.

2.3 Phonon glass-electron crystal (PGEC)

We know that thermoelectric research had led to the discovery of new materials with improved properties. The first useful pointers are the thermal conductivity (κ_l) decreases with increasing average atomic weight. It is also suggested that the ratio of carrier mobility (μ) to lattice conductivity increases with atomic weight. These ideas led to the selection of Bismuth Telluride as a thermoelectric material with a low value for κ_l, especially when it is mixed with isomorphous compounds.

The development of efficiency must have a low κ_l, which the filled-cage compound has received a lot of attention. The principle called phonon-glass electron-crystal (PGEC) that atoms are loosely bound in a large, atomic cage "rattling" which distributes heat to the acoustic phonon leads to low levels thermal conductivity “glass-like”, these materials have lattice thermal conductivities similar to amorphous materials but have electronic structures that can be described as for crystalline solids developed by Slack.(4) They believe that

electronic properties can reach modifications in this material, a great choice for efficient thermoelectric.

PGEC can be found among skutterudites, Zintl compounds and some clathrate with Seebeck coefficients in the order ± 200 mV/K or more and has a large power factor. For example, ZT = 1.1 has been detected for Eu-filled skutterudite at 700 K (1) and similar values for other skutterudites and some clathrate, although these materials have lower thermal conductivity than bismuth Telluride alloys but inferior to room temperature due to the relatively small power factor.

2.3.1 Skutterudites

Skutterudite is a type of thermoelectric material that was first discovered in Norway in 1845. It has received popular attention with its ability to dramatically reduce κ_l, which is facilitated by filling of cages within structures of heavier and smaller ions in the voids will have more abnormalities that are created, the decrease in κ_l of the lattice is even greater.(6)

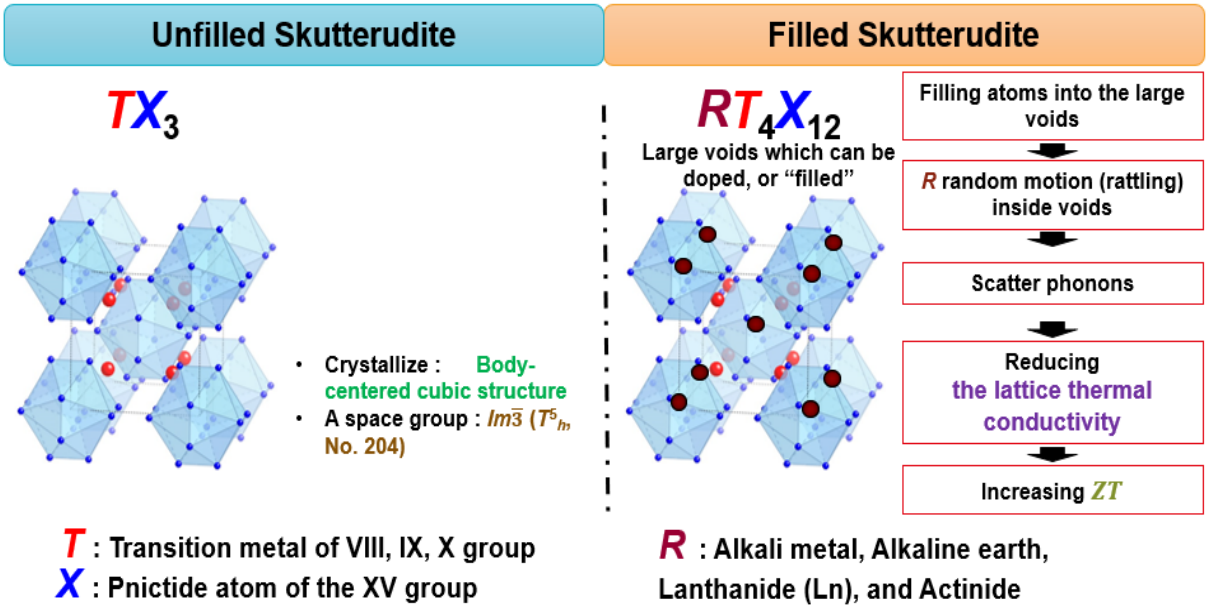

Figure 2.3.1. Unfilled and filled-skutterudite structure.

Figure 2.3.1 shows the unfilled-skutterudite structure is a cube (with the $Im\bar{3}$ space group (T_h^5, No. 204)) and the cell unit has eight TX_3 groups, where T is the transition metal element of VIII, IX, X group such as Fe, Ru, Os, Pt, X is Pnictide atom of the XV group such as P, As, Sb, Ge. It has 32 atoms per unit cell, one unit by metal atoms at an angle of eight cubes (with six (4 atoms) Sb rings inside the cubes with two voids in the remaining cubes. In the other is filled pattern for thermoelectric, the general crystal structure of these materials can be best described by RT_4X_{12}, which *R* is Alkali metal, Alkaline earth, Lanthanide (Ln), and Actinide, the existence of two voids in the structure, which are generally by atoms of rare elements creating the most pronounced effect of reducing the thermal conductivity.(1) Other metals and pnictide sites are doped to compensate for additional electrons from doping, a rare-earth (*R*), and to improve electronic properties. Reduction of the thermal conductivity of skutterudites that are caused rattling has a great impact on the propagation of the phonon through the lattice, attaching the 'rattlers" more loosely bound. Produce local vibration modes of lower frequencies, heat-carrying phonons.

In literature as shown a great performance of filled-skutterudites, $(Ce_yFe_{1-y})_xCo_{4-x}Sb_{12}$ at T = 1,000 K had a *ZT*=1.4 (6)**,** Yb partially filled skutterudites with *ZT*>1 at 600 K (4), A 19% Yb in $CoSb_3$ dramatically decreases κ_l as compared to the unfilled, $Yb_{0.19}Co_4\ Sb_{12}$ specimen has a low κ, higher than the estimated minimum κ of $CoSb_3$, κ_{min} = 0.3 W/mK. *ZT*~1.4 for p-type $DD_{0.6}Fe_3CoSb_{12}$ at 800 K and *ZT*~1.9 for n-type $(Sr, Ba,Yb)_yCo_4Sb_{12}$ at 835 K (7) As shown in these examples, both p-type and n-type filled skutterudite compounds can be synthesized depending on the filling ratio of *R* atom and the partial substitution of *T* atom.

2.3.2 p-type and n-type filled skutterudite compounds

The thermoelectric module (TEM) consists of a thermoelectric connection of p- and n-type in series by a lead strip (usually copper), this basic unit can still use as a building unit for the construction of a thermoelectric conversion system. A less complicated way for system engineers is to use TEM is building block as shown in Figure.2.3.2, the number of basic units connected by electricity in the series. But the heat in parallel and sandwiches Between two ceramic plates. TEM can be completed for products in various dimensions.

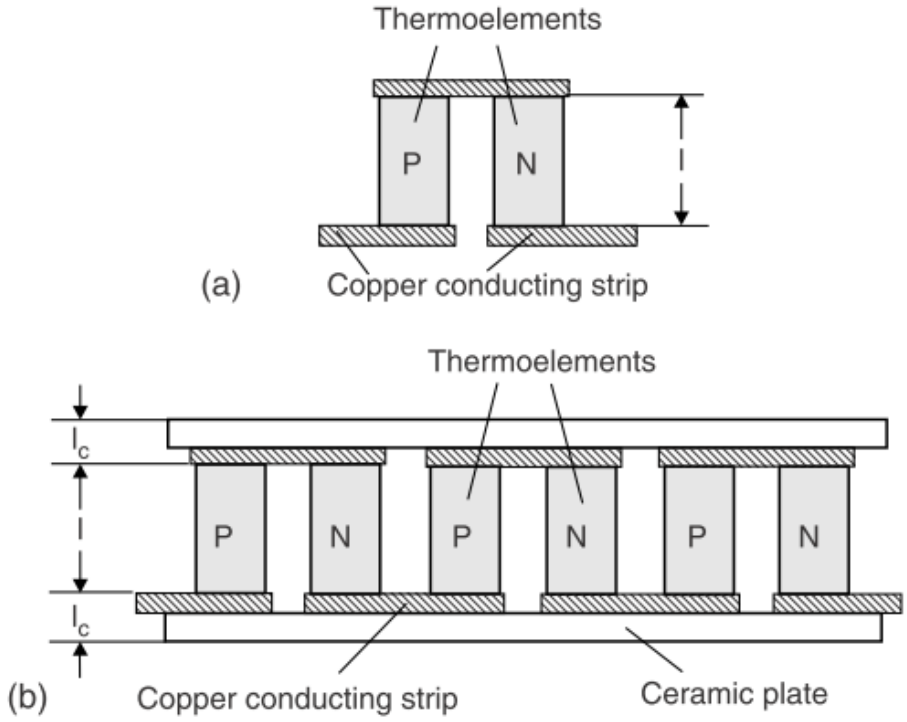

Figure 2.3.2. The basic configuration of TEM (a) basic unit, and (b) realistic model.

In literature, p-type skutterudites originated from the binary compound $CoSb_3$ and shown high-performance *ZT* value. The partial or total substitution of Co with other transition metals such as Fe and Ni provided that the electron count rule.(1) The successful synthesis of many *R*-filled $R_y(Fe_{1-x}Ni_x)_4Sb_{12}$ skutterudite compounds, the p-type skutterudites with maximum *ZT* value reaches 0.8 for $Ce_{0.9}Fe_{3.9}Ni_{0.1}Sb_{12}$ at 800 K sample prepared by a traditional solid-state reaction method(8), the p-type skutterudite with maximum *ZT* value of 0.16 for $Tl_{0.6}Fe_{2.5}Ni_{1.5}Sb_{12}$ at 422 K sample prepared by a quenching and annealing method(9), the n-type skutterudite had *ZT* reached values higher than 1 for $DD_{0.76}Fe_{3.4}Ni_{0.6}Sb_{12}$ at temperatures above 650 K sample prepared by a melting reaction technique, quenching, and annealing method.(10) In addition, literature has been reported Sm fillers atoms get the attention of donating electrons to the crystals had improved *PFs* and κ_L value by rattling effect. In order to separately produce p-type and n-type skutterudites with high *ZT* values, we have to carefully

tune the carrier concentration and filling ratio of *R* atom. Recent studies of Fe/Ni based skutterudites $Sm_y(Fe_{1-x}Ni_x)_4Sb_{12}$ indicated the p/n crossover at around x = 0.37 and y = 0.31. In this system, high *ZT* value of 0.55 at 560 K has been reported (11), as shown in Figure. 2.3.3. and Figure. 2.3.4

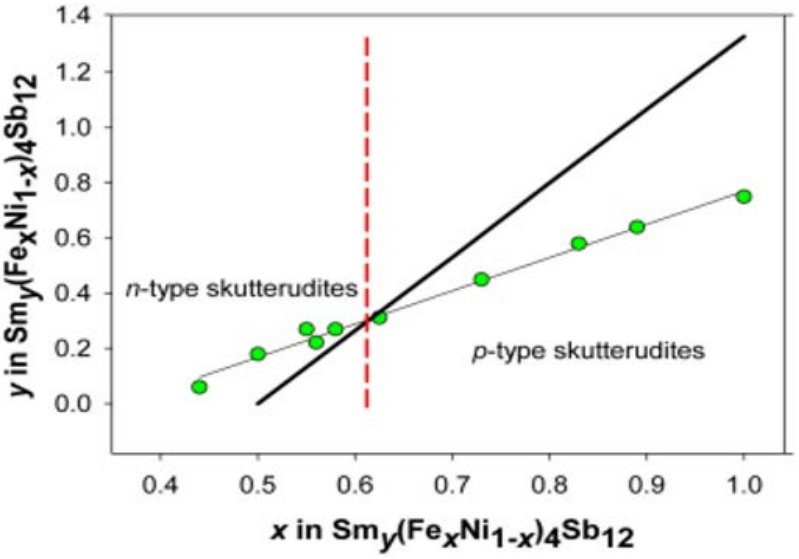

Figure 2.3.3. The p/n crossover of direct reaction of the elements at 1223 K, followed by quenching and subsequent sintering at 873 K.

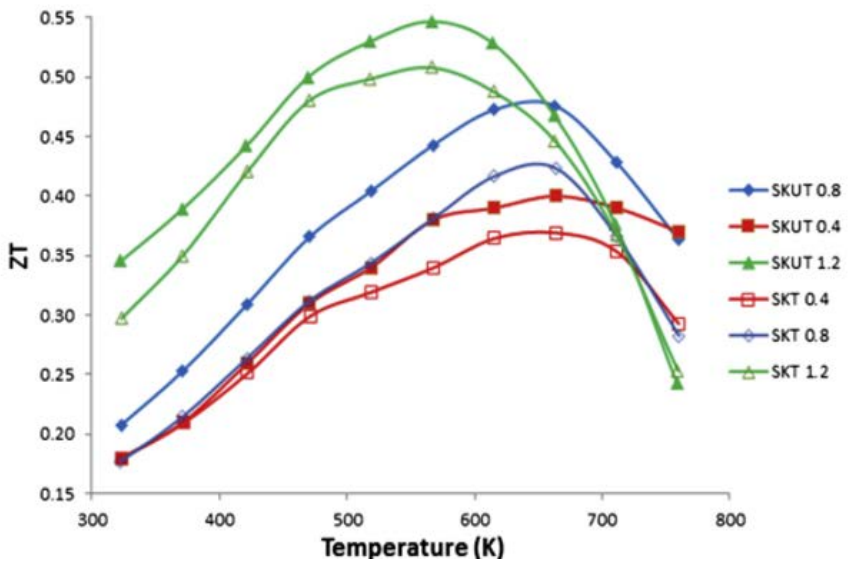

Figure 2.3.4. p-type of $Sm_y(Fe_{1-x}Ni_x)_4Sb_{12}$ prepared by $Sm_y(Fe_{1-x}Ni_x)_4Sb_{12}$ prepared by A quick melting, an annealing. (SKUT series: A quick melting, an annealing at 903 K for 7 days, and SKUT series: A quick melting, an annealing at 873 K fo 2.5 days)

The potential *ZT* should be achieved by carefully expanding the areas of synthesis with the tune the Sm filling ratio, also the Fe/Ni substitution around the p/n crossover area is attributed to the increase of *S* values. The TE properties can be tuned by the Sm-filled and the substitution Fe/Ni content, investigated the TE properties of p-type and n-type filled skutterudites $Sm_y(Fe_{1-x}Ni_x)_4Sb_{12}$ prepared by HPS technique, which this method helps to usually take a few hours, estimated a decrease in synthetic temperature and the densification rate can be improved by pressure, such as the relaxation of the n-type defects, a reduction in grain size (12) to reduce κ values, power factor (*PF*) resulting in improved TE properties, the concentration of high the Sm-filled, also obtaining material properties more rapidly, and cleanly than the other chemical techniques.

2.4 High-pressure synthesis technique

High-pressure synthesis is a technique that can adjust the structure and properties of the material resulting in the synthesis of new materials. The most commonly used high-voltage high-temperature technique (HPHT) consists of a synthesis of a high-voltage balanced phase that can be maintained after the voltage is released. In many cases, at medium temperatures, the voltage conversion causes kinetic energy to be correlated in a thermodynamically stable area in the pressure and temperature diagram (P, T).(12) HPHT is important laboratory-scale high-pressure tool, Bridgeman and Pistons have been developed to synthesize excellent materials that are pressured by more than 5 GPa with a volume of about 1 cm^3. They can reach a maximum pressure of 3 GPa at a volume of less pressure zones. Bridgeman anvil can accept very high voltages depending on the type of anvils, anvils hard alloy, the pressure ranges from 15-20 GPa, the SiC anvils for 20–70 GPa, and diamond anvils for 100–300 GPa. A commercial press machine that combines the concepts from anvil design. The high voltage instrument in laboratory is the anvil diamond cell (DAC) is used extensively for surveying high pressure synthesis and for the analysis of material properties under high pressure reach to 150 GPa, and can be heated easily by using infrared laser that has over temperature 5,000 K.

The advantage of HPHT was a modify the micro and macro structure of materials at the nanoscale and particle level, such as grain size, surface morphology, structure, defects and concentration that means morphology (12),(13) and the structure of the material can be easily handled by changing conditions P,T, the amount of High-voltage materials have demonstrated an interesting characteristic among them, superconducting conductors, semiconductor, optical, electron transport, heat and dielectric, tuning pressure, and obtaining material properties quickly and thoroughly, while compared to chemical techniques.

The change in entropy involves relatively small volume change, which makes maintenance pressure easier than temperature. HPHT helps to produce the same material as atmospheric pressure by adjusting chemicals such as adding a mesh host with small atoms.(13) To stimulate the pressure of chemicals that create high pressure.

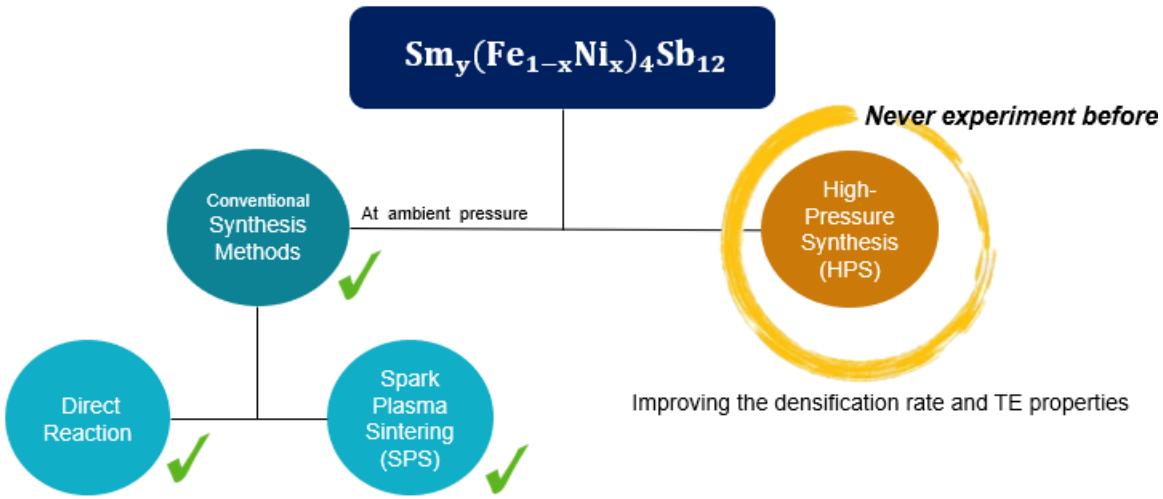

Figure 2.4.1. The high-pressure synthesis (HPS) for $Sm_y(Fe_{1-x}Ni_x)_4Sb_{12}$ sample.

Figure. 2.4.1 shows, the high-pressure synthesis (HPS) using multiple pressures can overcome this problem. This method allows increasing the filling part of the *R* atom in the skutterudite structure that is filled in comparison with the conventional methods. These substances have never been prepared using high-pressure synthesis techniques (HPS) before, which this method helps to usually take a few hours, estimated a decrease in synthetic temperature and the densification rate can be improved by pressure, such as the relaxation of the n-type defects, a reduction in grain size to reduce κ values, power factor (PF) resulting in improved TE properties, the concentration of high the Sm-filled, also obtaining material properties more rapidly, and cleanly than the other chemical techniques.

2.5 References

1. Rowe EDM, Ph D, Sc D, Group F. HANDBOOK. 2006.

2. Yushanov SP, Gritter LT, Crompton JS. Multiphysics Analysis of Thermoelectric Phenomena Thermoelectric materials • Behavior described by effect: October. 2011;0(1):1–18.

3. Rull-Bravo M, Moure A, Fernández JF, Martín-González M. Skutterudites as thermoelectric materials: Revisited. RSC Adv. 2015;5(52):41653–67.

4. Nolas GS, Morelli DT, Tritt TM. Skutterudites: a phonon-glass-electron crystal approach to advanced thermoelectric energy conversion applications. Annu Rev Mater Sci. 1999;29:89–116.

5. Hall EH. On a New Action of the Magnet on Electric Currents. Am J Math. 1879;2(3):287.

6. M. Tritt T. Thermoelectric Materials : Principles , Structure , Properties , and Applications. Encycl Mater Sci Technol. 2002;1–11.

7. Rogl G, Grytsiv A, Royanian E, Heinrich P, Bauer E, Rogl P. New p- and n-type skutterudites with ZT > 1 and nearly identical thermal expansion and mechanical properties. Acta Mater. 2013;61(11):4066–79.

8. Tan G, Zheng Y, Yan Y, Tang X. Preparation and thermoelectric properties of p-type filled skutterudites $Ce_yFe_{4-x}Ni_xSb$ 12. J Alloys Compd. 2014;584:216–21.

9. Choi S, Kurosaki K, Ohishi Y, Muta H, Yamanaka S. Thermoelectric properties of Tl-filled Co-free p-type skutterudites: $Tl_x(Fe,Ni)_4Sb_{12}$. J Appl Phys. 2014;115(2).

10. Rogl G, Grytsiv A, Bauer E, Rogl P, Zehetbauer M. Thermoelectric properties of novel skutterudites with didymium: DDy(Fe1-xCox)4Sb12 and DDy(Fe1-xNix)4Sb12. Intermetallics. 2010;18(1):57–64.

11. Carlini R, A. U. Khan, Ricciardi R, Mori T and Zanicchi G, J. Alloys Compd. 2016;655:321-326.

12. Drahansky M, Paridah M., Moradbak A, Mohamed A., Owolabi F abdulwahab taiwo, Asniza M, et al. We are IntechOpen , the world ’ s leading publisher of Open Access books Built by scientists , for scientists TOP 1 %. Intech. 2016;

13. Taylor P. High Pressure Research : An High-pressure synthesized materials : treasures and hints. 2007;(June 2012):37–41.

Chapter 3 Experimental methods

3.1 The high-pressure synthesis (HPS)

From the previous chapter 2 Let us know that rapid progress in technology, which has greatly improved the pressure and temperature of the experiment in research. There are many levels of pressure scales from 0.1 - 500 GPa or more. Creating a variety of high-pressure conditions for the exploration and synthesis of materials requires dynamic and static compression techniques that are different from press time. There are many physical phenomena that can be used in high voltage techniques such as thermal expansion and phase change. High-pressure synthesis (HPS) technique, in which the volume of the sample decreases when the bearing is pressed and the high pressure generated within the sample as long as the compression is large enough and the pressure can be maintained for a long time.(1)

The skutterudite compounds of p-type and n-type $Sm_y(Fe_{1-x}Ni_x)_4Sb_{12}$ were prepared high-pressure synthesis (HPS) technique by the cubic-anvil apparatus a DIA-type of Sumitomo Heavy Industries (UHP500).(2) The samples of $Sm_y(Fe_{1-x}Ni_x)_4Sb_{12}$ (nominal composition $0 \leq x \leq 0.56$, $0.1 \leq y \leq 1.2$) were prepared by the following two methods. The first one (Method I) was performed by direct reaction of pure elements samarium (Sm, 99.9%), iron (Fe, 99.99%), nickel (Ni, 99.99%) and antimony (Sb, 99.9999%) in quartz ampoules through the conventional melting-quenching-annealing technique; the obtained samples were subsequently ball-milled. They were mixed and sealed in a crucible fabricated of BN, and then assembled in a cubic pyrophyllite of 16 mm^3, as shown in Figure. 3.1.1., and the sintering conditions were 2 GPa and 500 ^oC. The second one (Method II) was the synthesis by direct reaction of stoichiometric amounts of high-purity elements Sm,

Fe, Ni and Sb using HPS technique, the synthesized pressure was 2 GPa and the reaction temperature was 430 - 490 ^{o}C for 120 min.

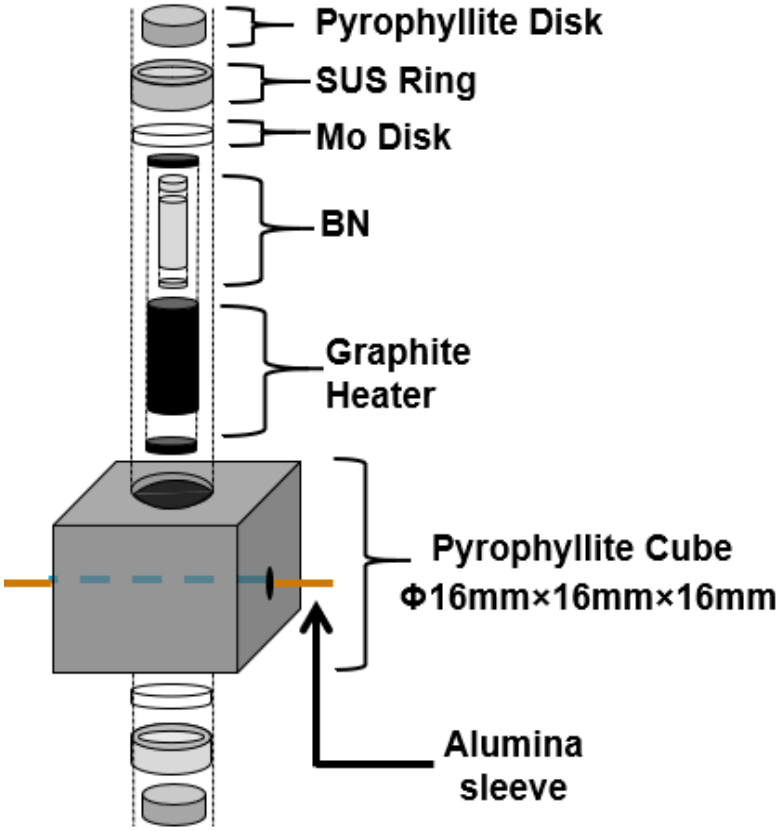

Figure 3.1.1. Assembly for UHP-500 synthesis.

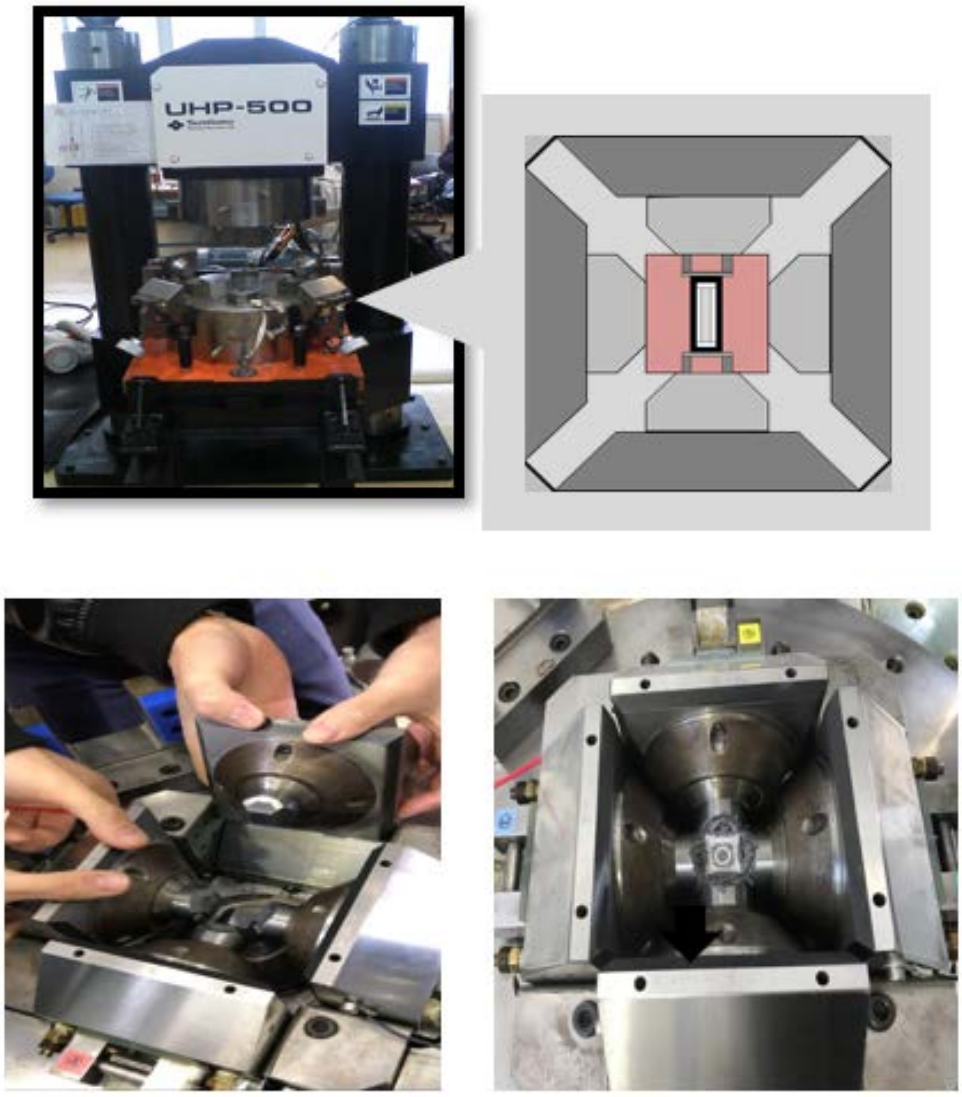

Figure 3.1.2. DIA-type high-pressure apparatus UHP-500 and the assembled anvil module.

DIA-type high-pressure apparatus UHP-500 and the assembled anvil module, as shown in Figure. 3.1.2., Anvil cube modules consist of 6 anvils made by tungsten carbide and 4 guide blocks with a 45^0 inclined plane. The upper and lower anvil are fixed, while the other 4 anvils are clamped on the 4 lead blocks, it can slide on the wedge. Each anvil has a face size 12×12 mm^2. The scrolling of the bottom frame will press 4 anvils in a horizontal direction and press the hydrostatic can be built on

all 6 faces of a cubic pyrophyllite. The oil pressure system is controlled by pressing in advance, maintaining pressure and reducing pressure patterns. The heating system is achieved by means of heating the AC current pass from the anvil, stainless steel rings, and Mo disks with high temperatures that can be operated between graphite. The hole is drilled, detects the temperature by inserting a thermocouple. The temperature inside a cubic pyrophyllite container of 16 mm^3 will rise.

3.2. Powder X-ray diffraction: XRD

X-ray diffraction analysis (XRD) is a general technique for studying crystal structures and atomic distances using creative infiltration of single X-rays and crystal samples. It is one of the methods for analyzing microstructure used for the crystallization. X-rays occur whenever high-speed electrons collide with metal targets. Therefore, any X-ray tube must have an electron source, an accelerating voltage, and a metal target. In addition, since the kinetic energy of most electrons is converted into heat in the workpiece, water is cooled to prevent thawing. All X-ray tubes consist of two electrodes, anode, with some exceptions, where the potential of the soil and the cathode is still at a high level, with the typical negative potential of about 30,000 to 50,000 volts for diffraction. X-ray tubes may be divided into two basic types according to the method that provides electrons, there are a gas pipe that produces electrons by making a small amount of gas, and incandescent bulbs.(3)

Figure 3.2.1. XRD (RINT RAPIDII(Rigaku)).

In this work, the samples were characterized by powder X-ray diffraction analysis (RINT RAPID II (Rigaku)) using Co$K\alpha$1 radiation and silicon as a standard at room-temperature for phase identification of crystalline material, as shown in Figure. 3.2.1.

X-ray reflection, according to Bragg's crystal law is fired with X-rays of a fixed wavelength, and at some point, in the incident, the strongly reflected X-rays will occur when the wavelengths of scattered X-rays. The path must be equal to a multiple of a wavelength. When interference occurs, the scattering beam of the X-rays causes the crystal to be at an angle equal to the incident beam as shown in the equation below,

$$CD + BD = n\lambda \quad (1)$$

If CD = BD and $\sin\theta = CD/d$

$CB = d_{hkl} \sin\theta$

Therefore,

$$2\, d_{hkl} \sin\theta = n\lambda \qquad (2)$$

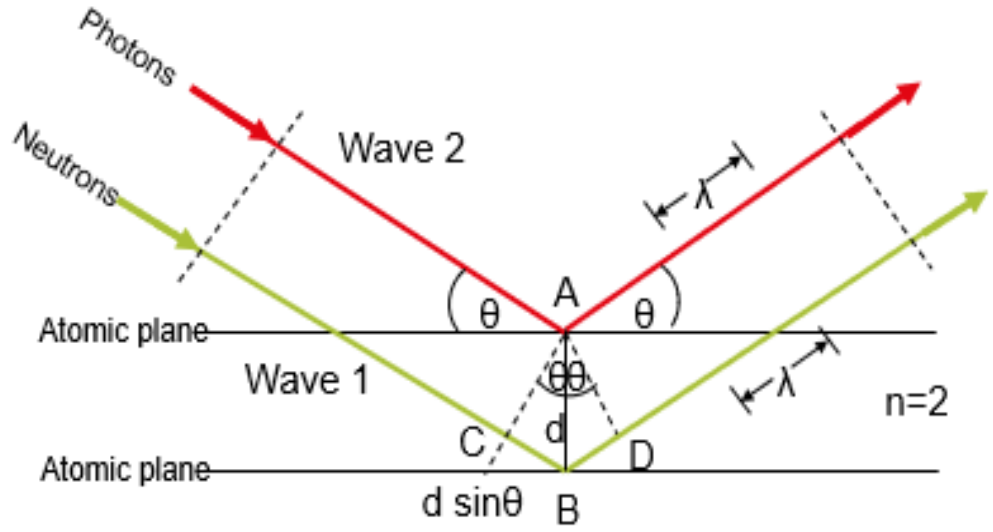

Figure 3.2.2. Bragg Diffraction Law.

Bragg's diffraction in Figure. 3.2.2 is a reflection of X-rays on the surface of the mirror imagery caused by the plane in the crystal. Due to the nature of the crystals repeatedly, these planes are separated by a constant distance d. Two X-ray beams of wavelength λ arrive at the top of the imaginary plane with the incident angle θ and form as waves. In order to get a common effect after reflecting the X-ray beam, both should remain in phase. (Green line on the right). The situation will only occur when the difference of the path traveled by wave fronts AC and AD (wavefronts before and after reflection) corresponds to the integer wavelength number. This condition is equivalent to saying that the sum of the CB and BD groups corresponds to an integer (n) times the wavelength (λ).(3)

3.3. Scanning electron microscope: SEM & EDX

Scanning electron microscopy (SEM) is an indispensable tool in research and industry. SEM had a deeper depth and resolution than optical microscopes that are suitable for observing complex morphology and surface height measurements. SEM had a wide magnification range for observation from an overall perspective similar to the naked eye to the nanostructure. SEM can install analytical capabilities to search for components in micron-level areas.

Energy dispersive X-ray (EDX) spectroscopy is involved in the investigation of the composition of the substance using a scanning electron microscope. EDX can detect elements with atomic numbers higher than boron and can detect these elements at a concentration of at least 0.1%. The application of EDX includes material evaluation and identification, contamination identification, analysis, spot detection of areas up to 10 cm in diameter, screening, quality control, and others. When colliding with an electron beam, in general, SEM, for example, works with the beam and produces X-rays. Due to the principle that none of the components have the same X-ray radiation spectrum, they can differentiate and measure the concentration in the sample.(3)

The interaction between electrons - matter, the interaction between matter - electrons beam generates a variety of signals with various information about the sample as shown in Figure 3.3.1., lustration of the electron-matter interaction depicting its different products. For example, the reflected electrons create a contrast image, which brings information about different atomic numbers. They can provide information about the electronic structure and chemical composition of the material and the electrons sent, can explain the internal structure and sample of other types of signal crystals that are widely used in SEM are X-rays.

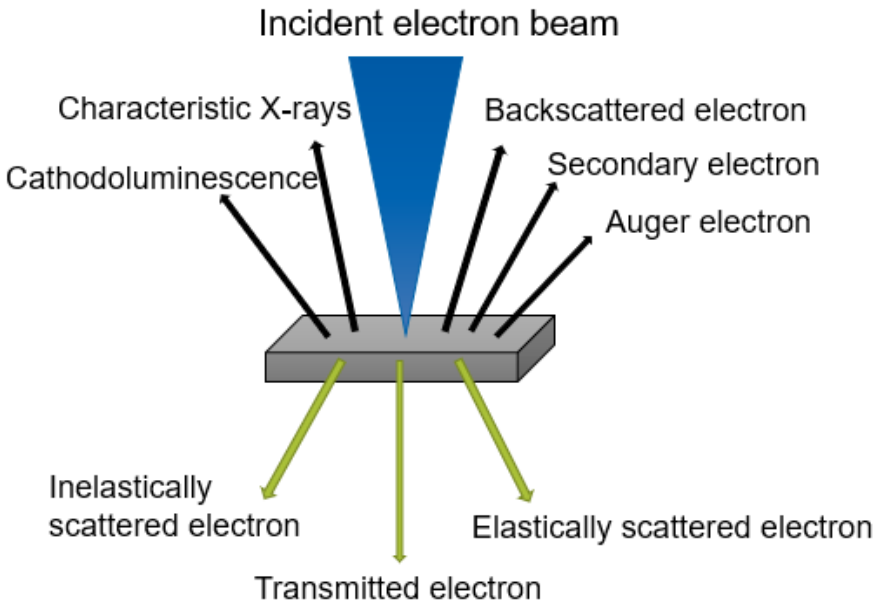

Figure. 3.3.1. lustration of the electron-matter interaction depicting its different products.

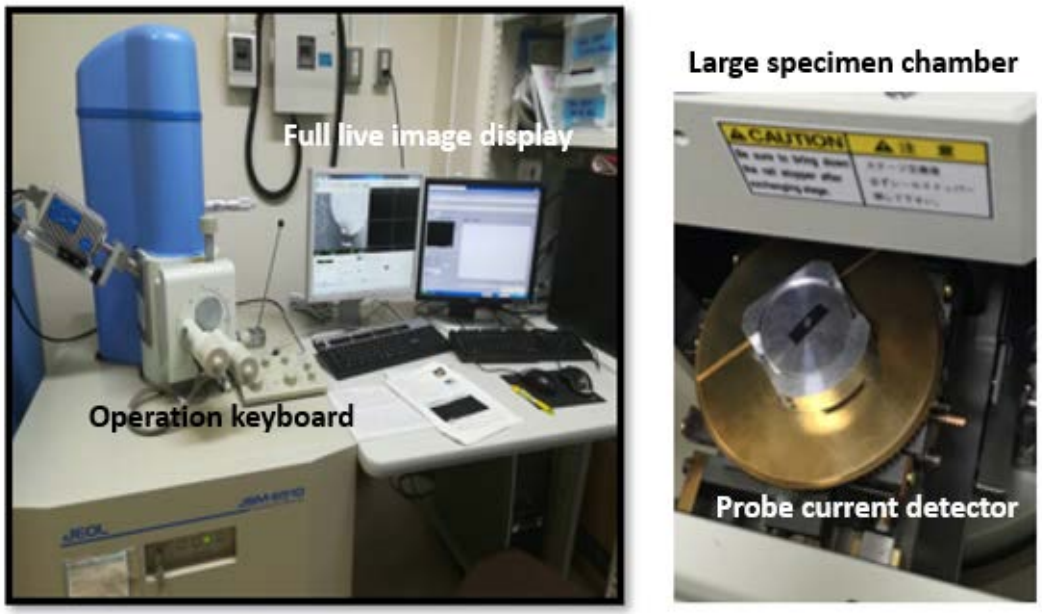

Figure. 3.3.2. SEM with energy dispersive X-ray Spectroscopy (EDX), JSM-6510 made by JEOL.

Operation of SEM with energy dispersive X-ray Spectroscopy (EDX/EDS), JSM-6510 made by JEOL as shown in Figure.3.3.2, all functions can be performed with the software, and show in a full live image on the display computer. We can add function keys as an option and use the adjustment function frequently by using the key on the operation keyboard. In the large specimen chamber, the condenser lens operation will adjust the probe current and focus during the probe current change. It makes it quick to increase the efficiency by the probe current detector.

For sample preparation, we will attach the sample in the cylinder with carbon tape, then combine it in the sampling process and insert it into the room. After that, we will click the HT icon to open the electron source, automatically adjust the current source and the camera image will appear on the operation screen. The image sharpness is higher than the probe current. However, damage from electron irradiation or heat increases. The current large probe reduces image resolution. But for the reflected electron detector their High sensitivity makes the electron detector reflect the image of the highly sensitive sample composition.

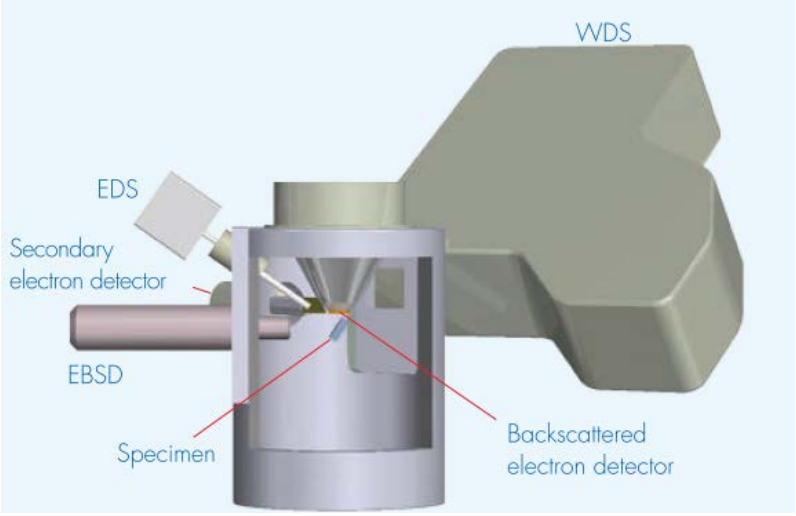

Figure. 3.3.3. Detector layout of JSM-6510 made by JEOL.

A wavelength dispersive X-ray analyzer (WDS) represent in Figure. 2.3.3, WDS has a resolution higher than EDS, nearby spectrum peaks which are not

modified by EDS. WDS are suitable for detecting an element of sample. EBSD analyzes the crystal orientation of crystalline materials. The EBSD detector is located below the EDS detector at 90 ° to the tilt axis of the specimen stage.(4)

In this work, the actual chemical compositional analysis was measured by scanning electron microscopy with energy-dispersive X-ray spectrometry (SEM-EDX). The nature of the SEM image will vary depending on the accelerating voltage, advice to choose the suitable voltage (Electron energy) for your specimen with the density and size of the structure. Normally, our laboratory uses 10 μm, 3,000 MAG. HV 15 kV WD 15 mm conditions with 8-10 different points all phase was analyzed.

3.4. Electron Probe Microanalyzer (EPMA)

A proto-type, electron probe microanalyzer (EPMA) is a tool to analyze the composition of substances by electron irradiation on the surface of the substance and the generated X-ray measurement, as shown in Figure.3.4.1. EPMA are designed and optimized for X-ray analysis of components from very small sizes. The accelerated electron beam that irradiates the specimen to create X-rays of secondary electron characteristics reflected electrons and other signal ranges. EPMA detects these signals, allowing images to be taken of samples, showing qualitative and mapping area results. Analyzing and mapping components in both micro and macro area.

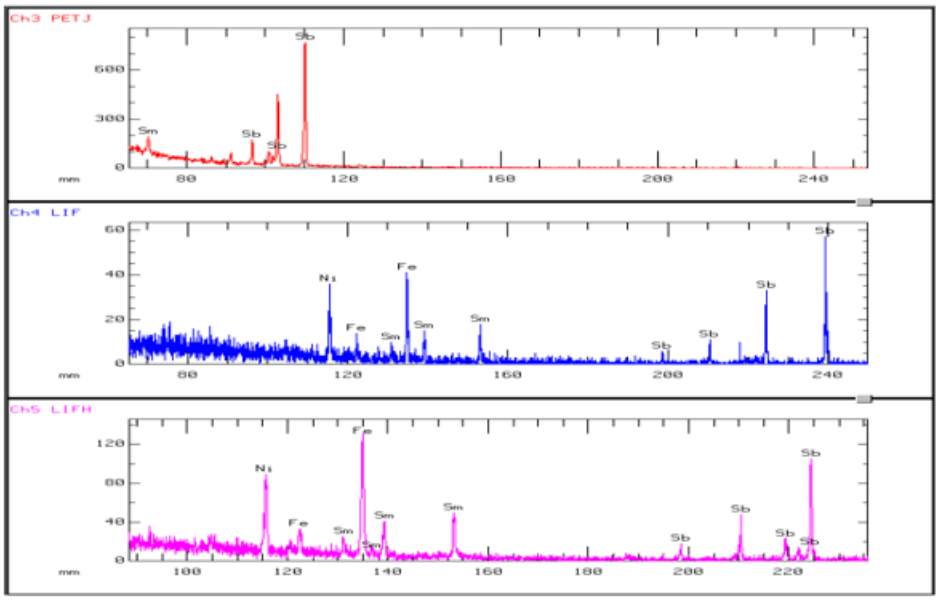

Figure. 3.4.1. The qualitative analysis (element spector).

Figure. 3.4.1 shows as, the qualitative analysis using independent high-speed spectrometer and high sensitivity crystal analysis can finish in one minute, the point-and-click analysis function makes it easy to use by specifying the analytical points on the SEM image combined with the use of the periodic table. The analysis range, just specify the desired range in the table. It can be calculated from spectral analysis from the spectra WDS database.

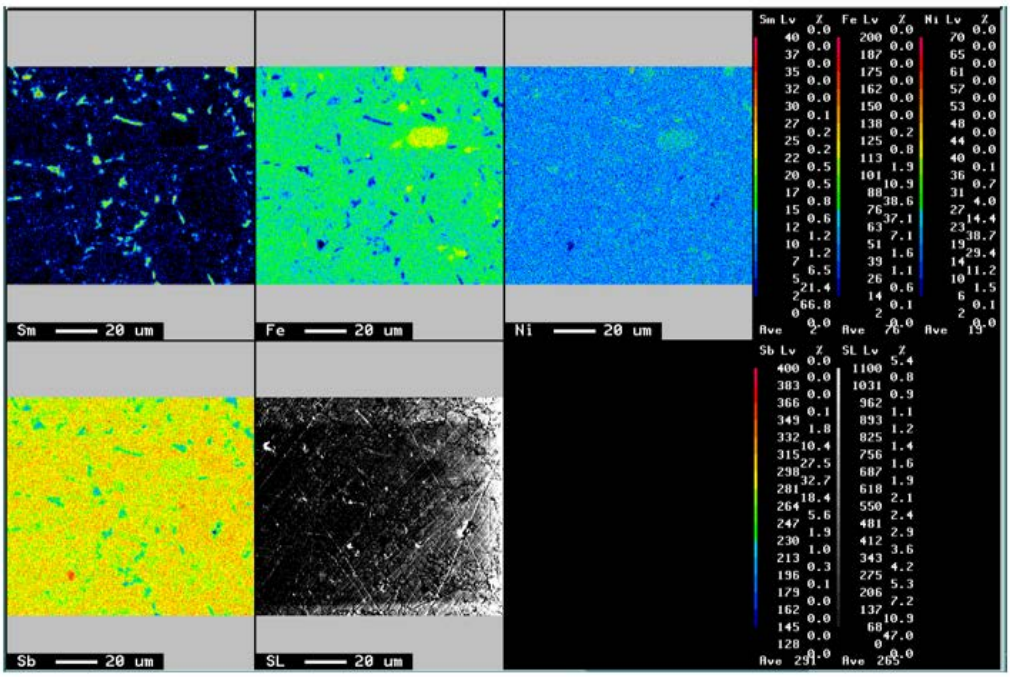

Figure. 3.4.2. The EPMA color mapping.

Figure. 3.4.2 shows the EPMA color mapping that has a range of micro to macro areas. The size largest is 90 mm. The most accurate mapping is possible to receive up to 5 data sets. The color display screen can be subdivided to be able to display up to 25 images at the same time and can rotate and display images in every angle. The color level can be changed, it also has functions for point analysis, line analysis in any direction, etc.

The instrument EPMA JXA-8900R made by JEOL is equipped with 4 X-ray diffused wavelengths. A wavelength dispersive X-ray analyzer (WDS) and energy dispersive X-ray Spectroscopy (EDX) combination can analyze up to 12 elements at the same time, collecting video signals from the backscatter and the secondary electron detector. The use of the WDS spectrometer is for a high detection sensitivity for tracking elements, accuracy in quantitative analysis, resolving power for adjacent X-ray spectra, and high accuracy in optical composition analysis.(5)

Figure 3.4.3. Overall, of EPMA, JXA-8900R made by JEOL.

Overall, of EPMA, JXA-8900R made by JEOL, as shows in Figure. 3.4.3, almost all the functions can be accessed from the software. However, the function also has access to the hardware from the console for convenience. There is an importance part are a monitor, console/control panel features, joystick control panel, optical microscope, and a workstation computer.

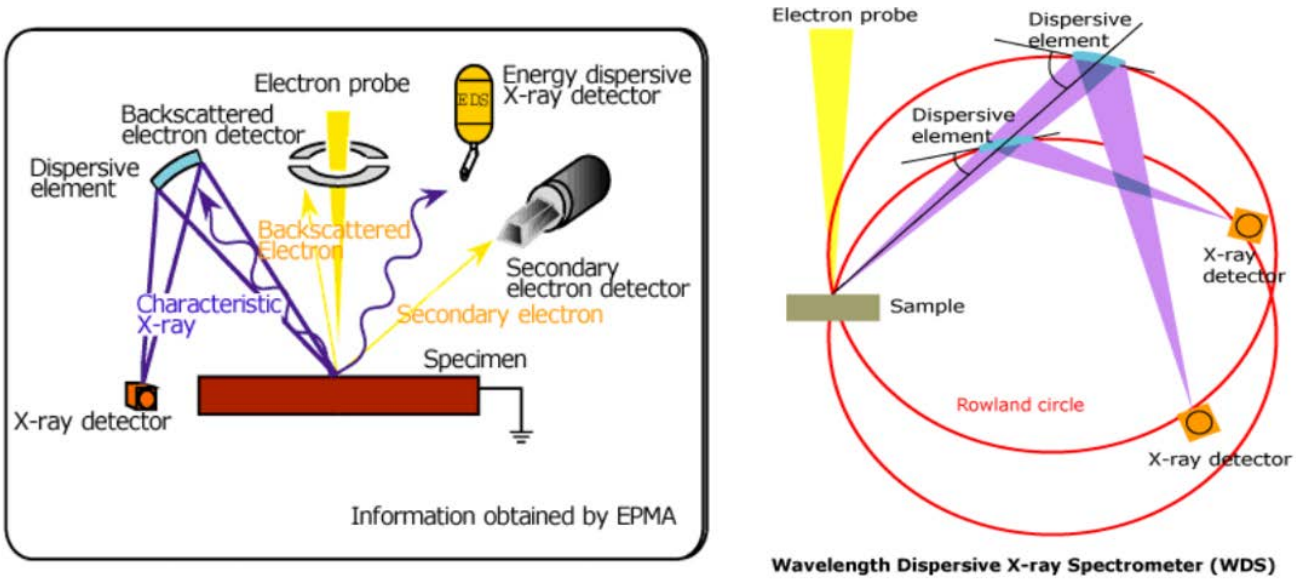

Figure. 3.4.4. Mechanism of EPMA (Electron Probe Microanalyzer).

The Mechanism of EPMA, when accelerated electrons hit a specimen, in addition to the X-rays, particles and electromagnetic waves carrying various kinds of information are emitted. EPMA signals such as the characteristic-X-rays, secondary electrons, backscattered electrons, etc. are detected by the appropriate detectors, and that data is used to find areas of interest on the specimen and for analysis.(5)

The electrons released from the electron source are accelerated by the accelerating voltage and are absorbed through the electron lens. An electron beam collides with a workpiece, the X-ray is created from the workpiece by using this X-ray distribution using the component distribution, the workpiece composition can be inspected. This type of spectrometer is called the X-ray wavelength dispersion spectrometer (WDS). WDS is constructed so that the specimen surface, analyzing crystal, and x-ray detector are positioned on a circle called the Rowland Circle, in order to satisfy Bragg's law, as shown in Figure. 3.4.2., mechanism of EPMA.

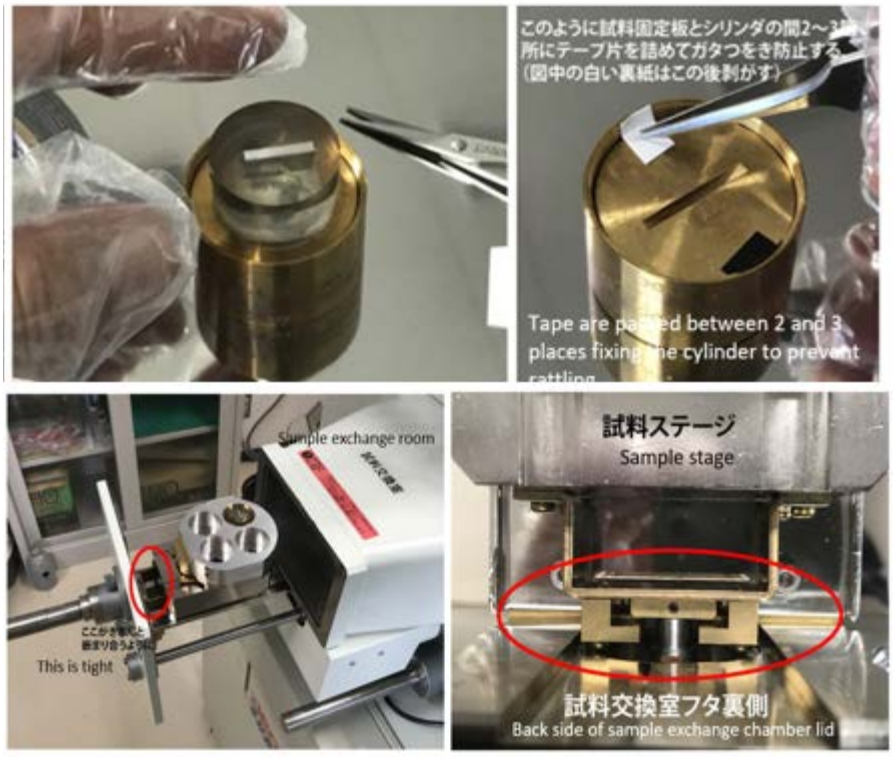

Figure. 3.4.5. The preparing samples.

In this work, the sample preparation is shown in Figure 3.4.5. The sample is attached to the cylinder with carbon tape, just like the SEM and EDX methods mentioned in the above. Then, we will be put in the sample exchange room by observing from the back of the sample exchange room followed in Figure 3.4.3., after that we will move to the next step. In our laboratory, we were analyzed 0,5,10 μm, 4-8 different points of qualitative analysis from the detected X-ray wavelengths.

3.5. Cryostat vacuum system

The electrical properties, resistivity (ρ) values were measured by a Cryostat vacuum system with a standard dc four-probe method. Four probe devices are one of the standard devices and are widely used to measure semiconductor resistance. This method is used when the sample is in the form of a thin sheet, such as a thin semiconductor material placed on the substrate, dc four-probe arranged in a straight line in a straight line at the same distance from each other. The sample should be adjusted to a group of squares (2.0mm×1.0mm×0.5mm) by polished with abrasive paper No. # 3000 and #8000, respectively. The area of another 4 surfaces must be calculated manually. To be used to fill in the program and software will calculate the value automatically.

As we know from Chapter 2, the semiconductor has a medium conductivity between the conductor and the insulation. The semiconductor differs from metals in the characteristic properties of reducing electrical resistance with rising temperatures, the semiconductor energy level can be divided into two bands, valence band and conduction band. In front of an external electric field, it is an electron in the valence ring that can move freely, therefore it is responsible for the conductivity of the semiconductor. In the case of semiconductors, the Fermi level is between the minimum of the thermal conductivity (κ) and the maximum of the capacitance. Therefore, electrical conductivity (σ) cannot be achieved at 0 K and the resistance is infinite as the temperature rises, the utilization rate of the conductivity strips increases, resulting in reduced electrical resistance (ρ) of the semiconductors.

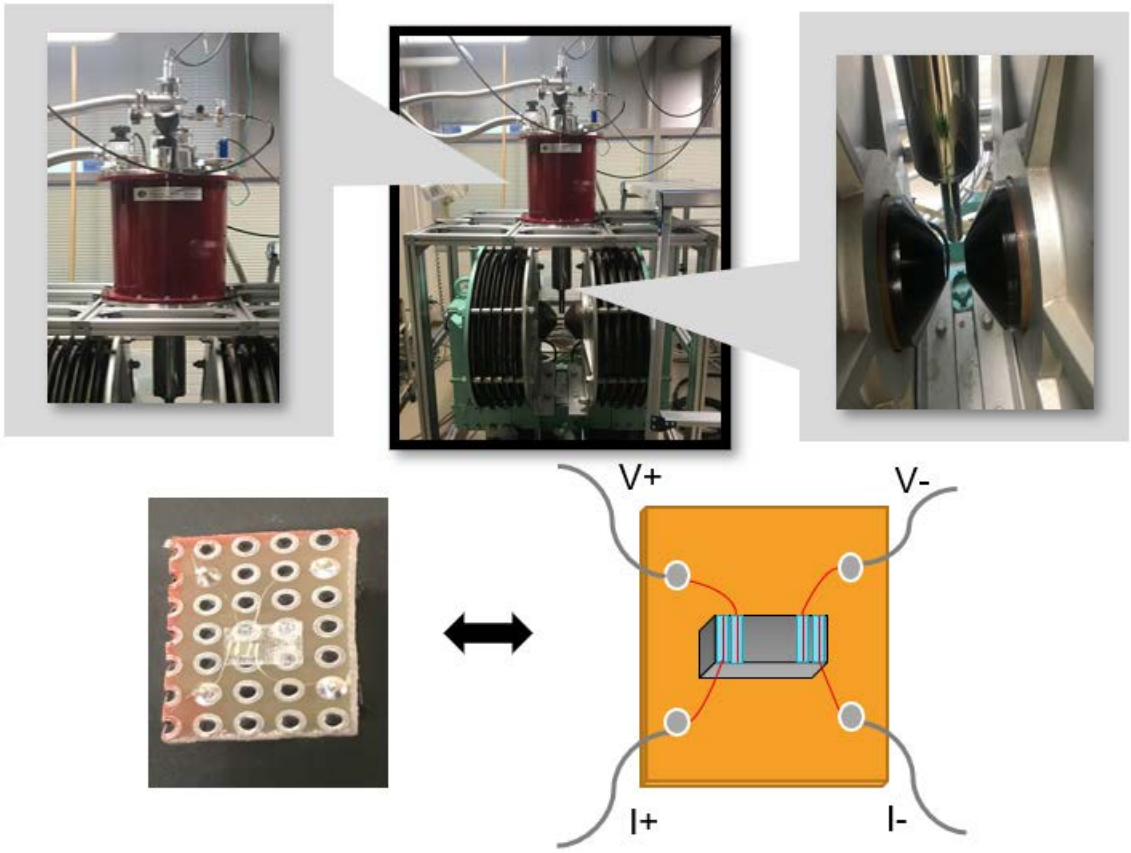

Figure. 3.5.1. Cryostat vacuum system and sample prepration with a standard dc four-probe method.

A constant current (*I*) is passed through two probes and releasing a possible (*V*) in two intermediate probes, as shown in Figure. 3.5.1. The cryostat vacuum system has a controller to heat the samples in order to study the behavior of the sample when the temperature rises, we used the temperature ranges conditions of measurement between 2 - 300 K.

Four probe methods, the material resistance is consistent in measurement. If there is a minority carrier injecting into the semiconductor, the electrodes with the most current of the service providers will reassemble near the electrode so that it will affect Little electrical conductivity. The surface of the probe head is flat without surface leakage, four probes used for contact surfaces, measuring resistance at points

in a straight line. The diameter of the contact between the metal probe and the semiconductor should be small compared to the distance between the probes. The boundary between the current-carrying electrode and the bulk material is a half-circle and smaller. The surface of semiconductor materials may be both operational and non-operational. The scope of operation is what materials with a much lower resistance than semiconductors are impregnated. Non-conductive boundaries occur when the surface of a semiconductor is in contact with the insulation.

3.6 Physical property measurement system : PPMS

Thermal properties, including a thermal conductivity (κ), seebeck coefficient *(S)*, and Hall effect were measured by The Quantum Design Thermal Transport option (TTO) for the Physical Property Measurement System (PPMS), as shown in Figure. 3.61

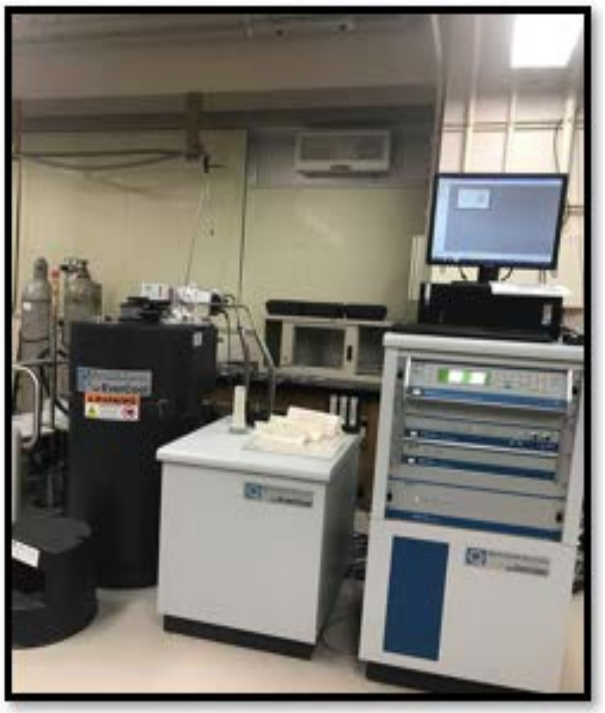

Figure. 3.6.1. Physical property measurement system (PPMS).

Thermal lattice conductivity (κ_l) values were calculated by subtracting κ values with thermal electrical conductivity (κ_e) values. All measurements can be used to calculate the *ZT* values in the temperature range of 2 K to reach room temperature.

3.6.1 TTO measurement

The TTO system measures the thermal conductivity or the ability of the material to conduct heat by checking the reduced temperature with the sample in the amount of heat known through the sample. TTO measures the effect of ground thermoelectric currents on the dropout voltage provided with reduced temperatures in some materials. They can measure both at the same time by checking both the temperature and the voltage drop in the sample. They use heat pulses at one end, the system can also measure electrical resistance by using the resistance of all four probes.

To measure the TTO, the samples should be modified to rectangular bulk (2.0mm×1.0mm×0.5mm), polished with abrasive paper (#3000 and #8000) and cleaned, it is can be same size with resistivity measurement, and then assembled with in thermal transport sample puck that connects to the three five-pin sockets on the green printed circuit board, as shown in Figure. 3.6.1.1.

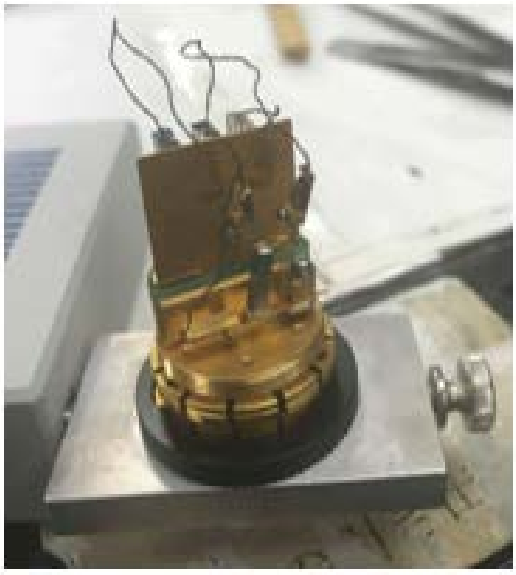

Figure. 3.6.1.1. Sample prepraration for TTO.

After that, checking the sample contact before measured, resistivity between V+/- and I+/- with an ohmmeter. The corresponding resistivity value should be, No.3-4 is around 200Ω, No. 5-6 is around 2 kΩ, No.7-8 is around 100Ω, No.9-10 is around 100Ω, No.11-12 and No.1-14 are show different resistivity value according to sample property, then move to the step of measurement.

TTO Option manager, as shown in Figure. 3.6.1.2, it can be select the Utilities-Activate Option menu command in PPMS MultiVu, select on option thermal transport, and then select Connection Diagram button.

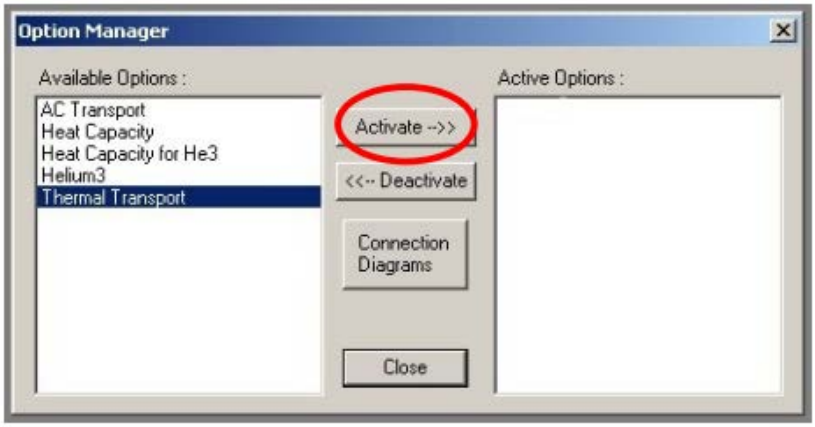

Figure. 3.6.1.2. TTO Option manager.

Before inserting the sample. It is necessary to set the inside of the chamber to 1 atm to control the pressure in the chamber, select the Vent Cont. at the Chamber state panel as shown in Figure. 3.6.1.3. Waiting until state become flooding, then insert the sample pack into the chamber using the sample insertion tool.

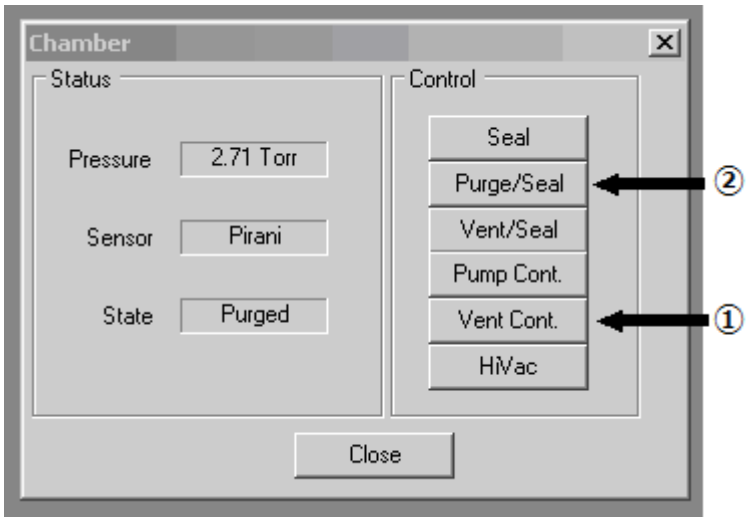

Figure. 3.6.1.3. Chamber Control.

Insert the contact baffle shielding cap tool in Figure. 3.6.1.4. into the chamber. Select Purge / Seal at the Chamber state panel, wait until the state becomes purged, and select High-Vac, then an active TTO option in software later.

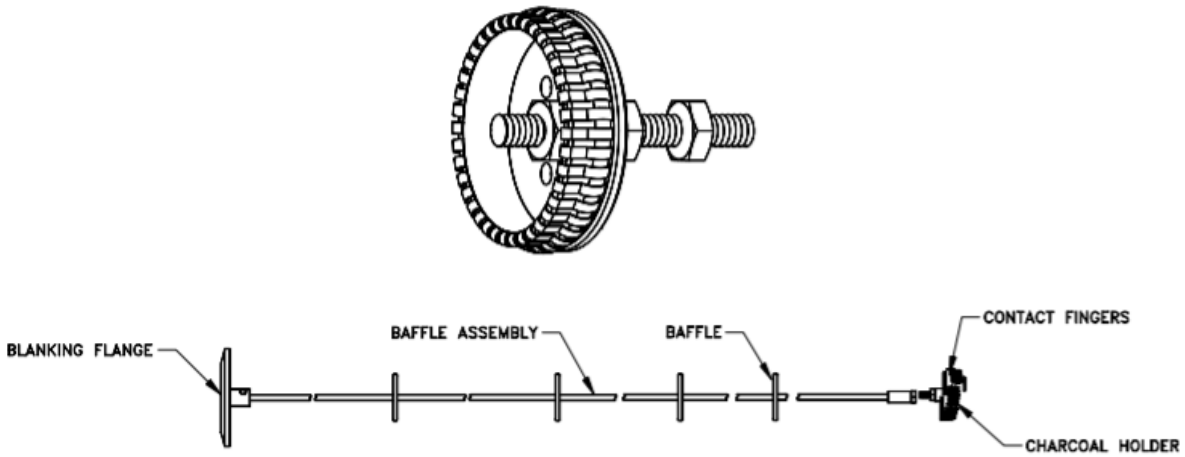

Figure. 3.6.1.4. Baffle assembly with contact baffle.

After that, it will be a measurement procedure within the program. The important part is the thermal transport waveform and the sequence writing according to the desired measurement conditions.

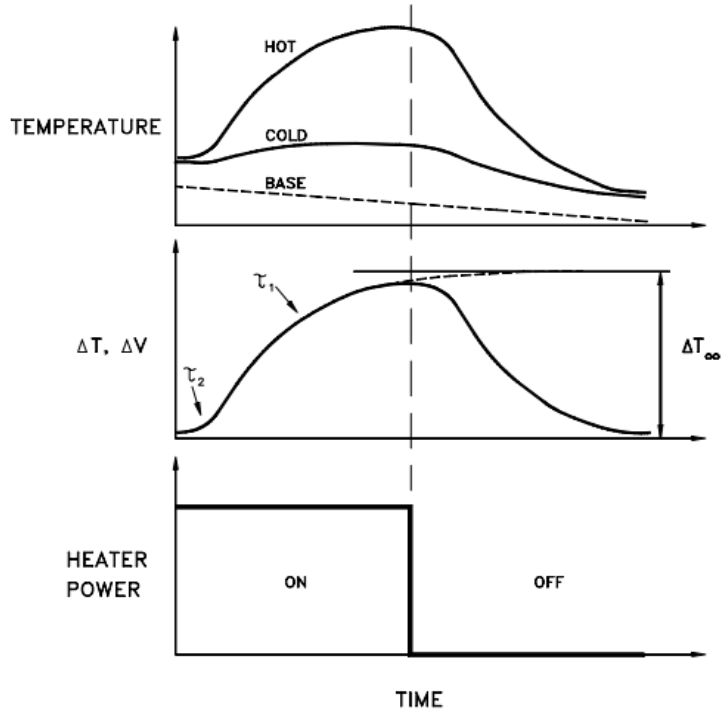

Figure. 3.6.1.5. Heat pulse and temperature and voltage response at hot and cold thermometer Shoes in an idealized Sample.(6)

Figure. 3.6.1.5., heat pulse and temperature and voltage response at hot and cold thermometer shoes in an idealized Sample, the top panel is a time tracking of hot and cold thermometer between ideal heat pulse Note that the PPMS base temperature fluctuates. The middle panel is corresponding temperature ΔT and voltage ΔV, the differential in the example shows the cooling time constant τ1 and τ2, the Bottom panel is the heater power between the square wave heat pulse. The sample should be shown a status normal waveform as same as a middle pane as shown in Figure. 3.6.1.5 before we would move to write a sequence for measurements.

3.6.2 Hall effect

Another function for PPMS, they can measure an electric resistivity for hall measurement, as we know that the energy factors of TE materials are adjusted to suit the carrier concentration (n) by measuring Hall effect from relating with $V_H = \frac{BIb}{neA} = \frac{R_H BI}{t}$, $R_H = \frac{1}{ne}$, where V_H is the Hall voltage (V), R_H is the Hall coefficient (cm^3/C), B is a magnetic field (Oe), b is the width of the sample and t is the thickness, and I is conventional current. The electrical conductivity is related to the carrier concentration as, $\sigma = n.e.\mu = 1/\rho$, where e is the elementary charge (1.6×10^{-19} C), μ is the carrier mobility are important for fully characterizing and understanding a TE material.

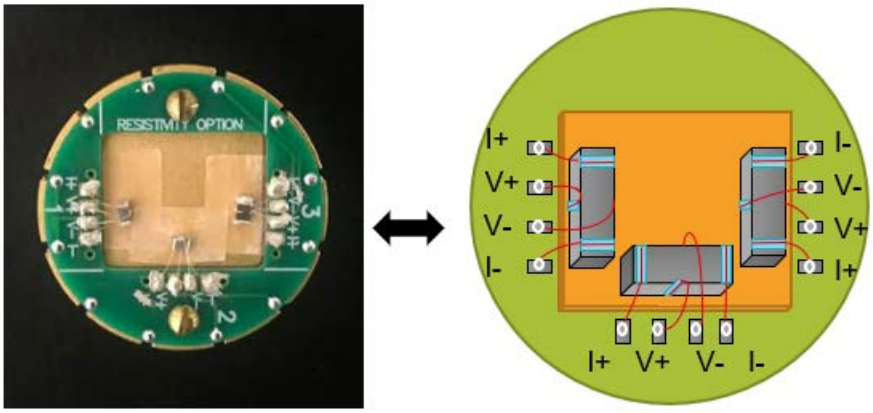

Figure. 3.6.2.1. Sample prepraration for Hall measurement.

Hall measurement, the sample size should be the same as TTO measurements, but the difference is we can assemble up to 3 samples per pack per measurement once, as shown in Figure 3.6.2.1, sample prepraration for Hall measurement.

In PPMS Option manager for hall measurement, we can be select the Utilities-Activate Option menu command in PPMS MultiVu, select on option resistivity for hall effect measurement, and then select Connection Diagram.

Before inserting the sample. It is necessary to set the inside of the chamber to 1 atm to control the pressure in the chamber, select the Vent Cont. at the Chamber state panel. Waiting until the state becomes flooding, then insert the sample pack in Figure 3.6.2.1 into the chamber using the sample insertion tool.

Insert the radiation shielding cap tool in Figure. 3.6.2.2. into the chamber. Select Purge / Seal at the Chamber state panel, wait until the state becomes purged, then an active resistivity option (Hall effect) in software later.

Figure. 3.6.2.2. Radiation shielding cap tool.

After that, it will be a measurement procedure within the program followed in detail.

1) The resistivity option is activated, the resistivity control, the screen in Figure 3.6.2.3, appears into the PPMS MultiVu interface. Then, create a data file. Press the Browse button in the resistivity control center Select the drive and directory.

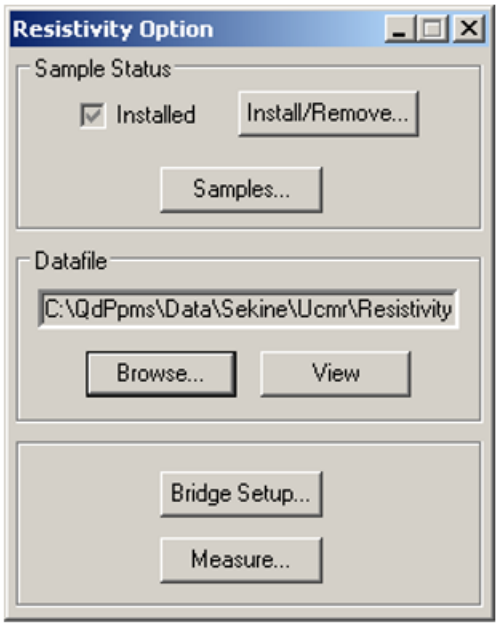

Figure. 3.6.2.3. Resistivity Option.

2) Enter the sample description to the File and Sample Properties dialog box opens, as shown in Figure. 3.6.2.4. The Sample description represents the user bridge channel that installed the sample.

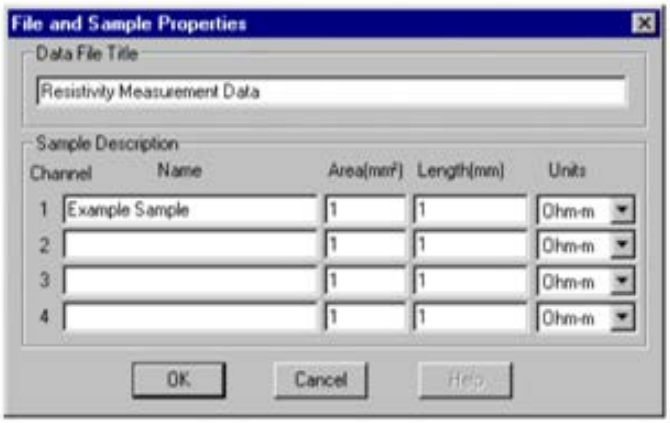

Figure. 3.6.2.4. File and Sample Properties dialog box.

3) Select Bridge Setup in Figure. 3.6.2.5., we will set from 5000, 3000, 2000, 1000, … in current limit (μA) for check resistivity in AC and DC mode in Drive mode, set power limit to1000 μV and Voltage limit to 95 mV to confirm that it is not an abnormal numerical value.

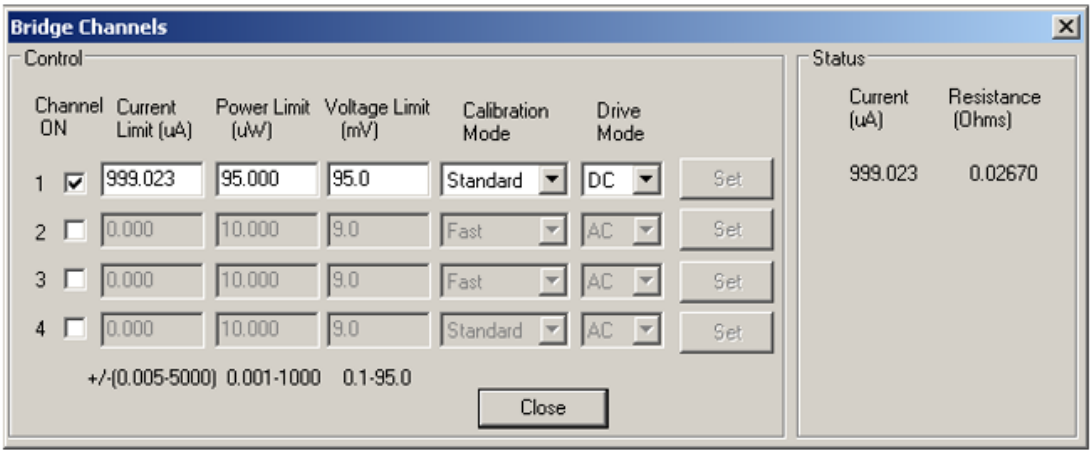

Figure. 3.6.2.5. Bridge Channels.

4) Write Sequence. And then Run sequence
5) Log. Open Utilities-Log PPMS Data by select Stop and then select Browse on the General tab, and create a new folder named Log in the folder. Within

the created new folder, set the File name as the date of the measurement date and make a file. Select Start.

6) Select View Data and Press Select All on all tabs, including the Standard Item tab, and take Log of all items.
7) In Figure. 3.6.2.6., Data Selection will select the item you want to display on this screen, then Figure. 3.6.2.7., it will be shown an axis.

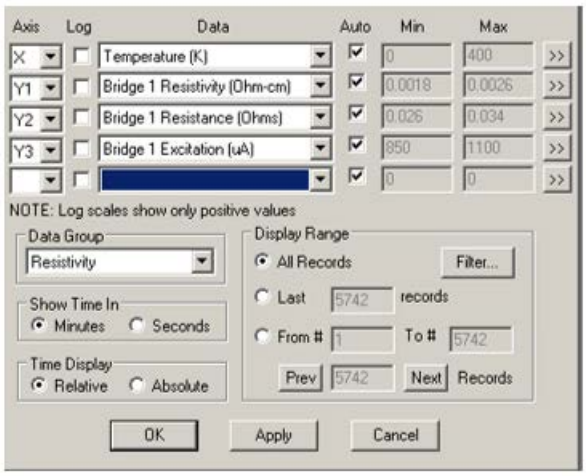

Figure. 3.6.2.6. Data Selection.

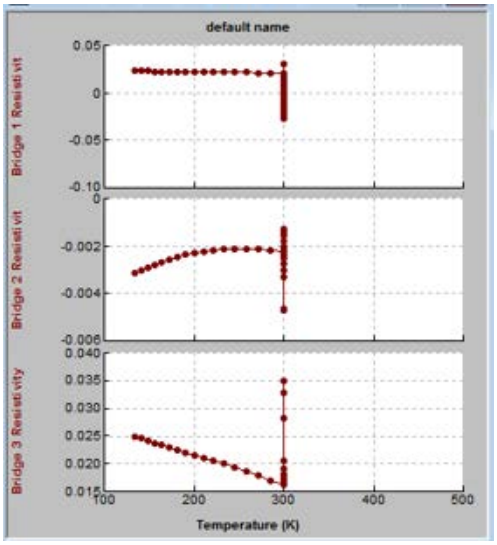

Figure. 3.6.2.7. Measurement screen.

After the measurement finish, the status in the left will become Sequence Idle. Ensure the chamber temperature is 300K. Then, open the chamber by click Vent Cont. Button. Then open the Dewar and take off the sample. Close the Dewar and click the Purge/Seal button to seal the chamber.

3.7 References

1. Liu XY. High Pressure Synthesis and Preparation of Inorganic Materials. Modern Inorganic Synthetic Chemistry: Second Edition. Elsevier B.V.; 2017. 105–141.
2. Sekine C, Mori Y. Development of thermoelectric materials using high-pressure synthesis technique. Jpn J Appl Phys. 2017;56(5):0–6.
3. B.D. Cullity and S.R.Stock. Elements of X-RAY DIFFRACTION Second Edition. Plant Management & Physiology. 1978. 569.
4. JEOL. JSM-6510 series. 2012;
5. Goodge J. Electron probe micro-analyzer (EPMA). Univ Minnesota-Duluth. 2012;2888.
6. Design Q. Physical Property Measurement System, Thermal Transport Option User' s Manual. Test. 2002;(1684):77.

Chapter 4 Results

4.1. Sample characterization

The skutterudite compounds of p-type and n-type $Sm_y(Fe_{1-x}Ni_x)_4Sb_{12}$ were prepared high-pressure synthesis (HPS) technique by the cubic-anvil apparatus a DIA-type of Sumitomo Heavy Industries (UHP500).(1) Firstly, the compounds were prepared by reacting stoichiometric amounts of High-purity elements samarium (Sm, 99.9%), iron (Fe, 99.99%), nickel (Ni, 99.99%) and antimony (Sb, 99.9999%) were mixed and sealed in a crucible fabricated of BN, and then assembled in a cubic pyrophyllite container of 16 mm^3. The samples were HPS with the approximately reaction temperature between 430 to 490 ^{0}C for 120 minutes under a pressure of about 2 GPa, are named **HP series**. For the conventional melting-quenching-annealing technique, the obtained samples were subsequently ball milled. Then, samples were sintered by using a cubic-anvil high-pressure apparatus (UHP-500, Sumitomo Heavy Industries). The sintering conditions were 2 GPa and 500 ^{o}C for 120 minutes, are named **ST series**, respectively. Bulk samples were achieved with the nominal content of $Sm_y(Fe_{1-x}Ni_x)_4Sb_{12}$, $0.1 \leq Sm \leq 1.2$, and $0 \leq Ni \leq 0.6$, respectively.

The samples were characterized by powder X-ray diffraction analysis (RINT RAPID II (Rigaku)) using Co$K\alpha$1 radiation and silicon as a standard at room-temperature for phase identification of crystalline material. The chemical compositional analysis was measured by scanning electron microscopy with energy-dispersive X-ray spectrometry (SEM-EDX) used to provide actual elemental identification analyses 10μm with 8-10 different points all phase was included, the point analysis of the qualitative analysis, and the color mapping technique (area analysis) from electron probe microanalyzer (EPMA), respectively. The lattice parameters (α) for the samples were calculated by the least-squares fitting method. Table I. displays the synthesis conditions of

$Sm_y(Fe_{1-x}Ni_x)_4Sb_{12}$ samples represent the nominal composition of samples, and results.

Table I. The synthesis conditions of $Sm_y(Fe_{1-x}Ni_x)_4Sb_{12}$ samples represent the nominal composition of samples, and results.

Samples			Conditions				Results
			Pressure [GPa]	Temperature [℃]	Power [W]	Time [min]	
ST1	$Sm_{0.8}Fe_{3.8}Sb_{12}$	#1	2	600	350	120	△
		#2		550	320		△
		#3		650	370		×
ST2	$Sm_{0.5}(Fe_{0.7}Ni_{0.2})_4Sb_{12}$	#4		510	290		○
ST3	$Sm_{0.3}(Fe_{0.6}Ni_{0.3})_4Sb_{12}$	#5		500	290		△
ST4	$Sm_{0.1}(Fe_{0.5}Ni_{0.4})_4Sb_{12}$	#6		480	280		×
ST5	$Sm_{0.04}(Fe_{0.4}Ni_{0.5})_4Sb_{12}$	#7		500	290		○
HP7	$Sm_{0.2}(Fe_{0.6}Ni_{0.4})_4Sb_{12}$	#8		600	400		×
		#9		550	380		×
HP1	$Sm_{0.2}Fe_4Sb_{12}$	#10		700	450		×
	$Sm_{1.0}Fe_4Sb_{12}$	#11		500	280		△
	$Sm_{1.2}Fe_4Sb_{12}$	#12		470	300		△
	$Sm_{1.2}Fe_4Sb_{12}$	#13		430	280		○
HP2	$Sm_{1.2}(Fe_{0.6}Ni_{0.4})_4Sb_{12}$	#14		450	280		○
HP3	$Sm_{1.0}(Fe_{0.6}Ni_{0.4})_4Sb_{12}$	#15		450	280		△
HP4	$Sm_{0.8}(Fe_{0.6}Ni_{0.4})_4Sb_{12}$	#16		450	280		△
HP5	$Sm_{0.6}(Fe_{0.6}Ni_{0.4})_4Sb_{12}$	#17		450	280		○
HP6	$Sm_{0.4}(Fe_{0.6}Ni_{0.4})_4Sb_{12}$	#17		450	280		○
HP7	$Sm_{0.2}(Fe_{0.6}Ni_{0.4})_4Sb_{12}$	#18		450	280		○

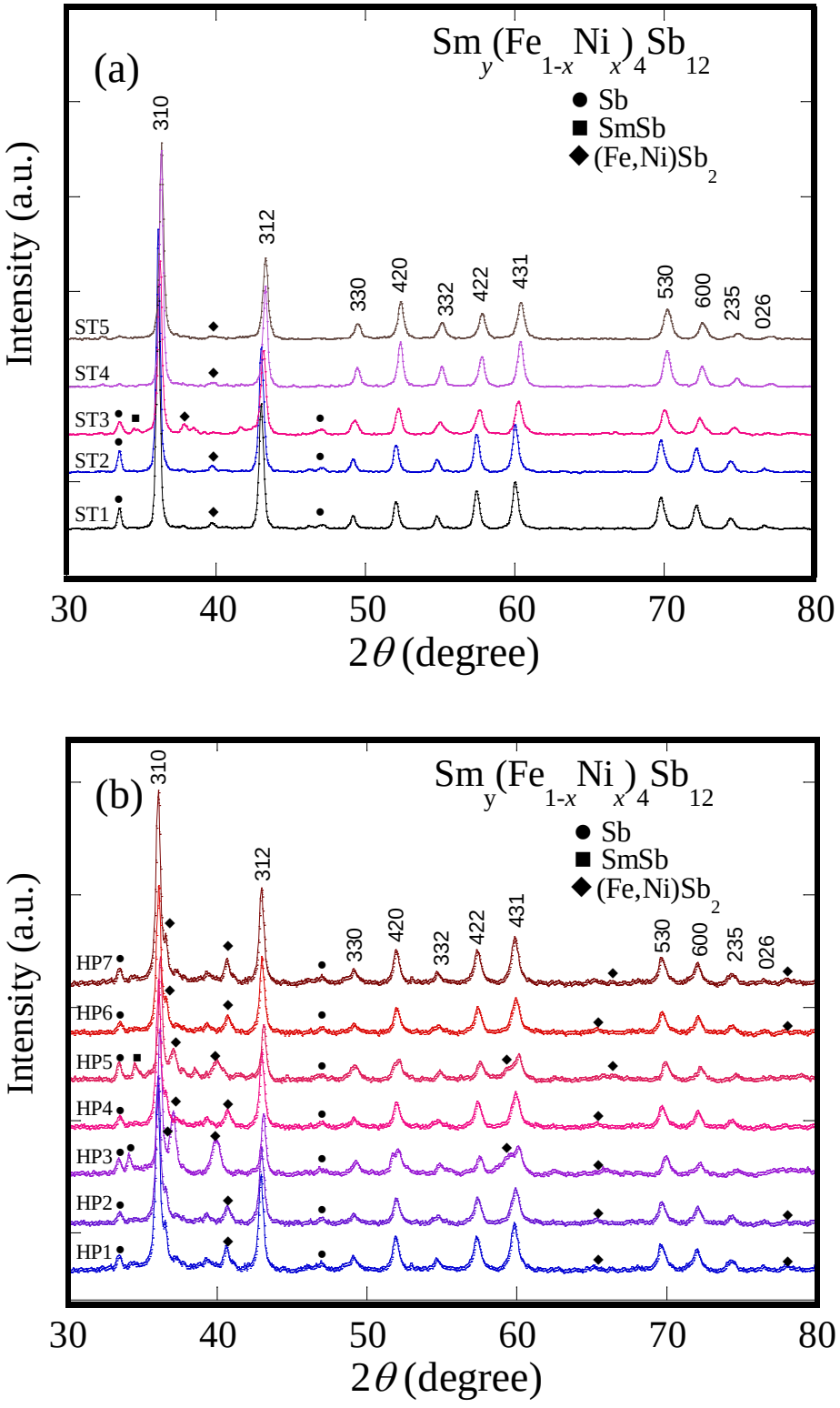

Figure. 4.1.1. Powder X-ray diffraction patterns of $Sm_y(Fe_{1-x}Ni_x)_4Sb_{12}$ samples (a) and (b) for ST series and HP series, respectively.

Powder X-ray diffraction patterns of samples can be observed in terms of the number of phases, $Sm_y(Fe_{1-x}Ni_x)_4Sb_{12}$ samples prepared under high pressure were measured at room temperature for phase identification of polycrystalline becomes p-type or n-type depending on composition (*x* and *y*) as shown in Figure. 4.1.1., powder X-ray diffraction patterns of $Sm_y(Fe_{1-x}Ni_x)_4Sb_{12}$ samples (a) and (b) for ST series and HP series, respectively. The results revealed a similar of filled skutterudites diffraction patterns due to the same space group of them ($Im\bar{3}$). The majority of the diffraction peaks revealed the homogeneity of $Sm_y(Fe_{1-x}Ni_x)_4Sb_{12}$ skutterudite phase as the main phase, and a few additional Sb, SmSb, and $(Fe,Ni)Sb_2$ phase were detected in almost every compound. The secondary phase in these compounds suggested the thermodynamically of them more stable than the skutterudite phase that the direct combination of addition atoms.(2) The influence of the impurity phase related to the TE transport properties as well.

The chemical compositions by the SEM–EDX analyses of $Sm_y(Fe_{1-x}Ni_x)_4Sb_{12}$ samples for HP and ST samples, as shown in Figure 4.1.2. SEM-EDX of $Sm_y(Fe_{1-x}Ni_x)_4Sb_{12}$ samples (a) and (b) for ST series and HP series, respectively, the results reveled images of polished and fracture surfaces have shown inhomogeneities. Samples have a many phase was observed by colors, the gray color is a skutterudite phase. the light gray color is a second phase also an Sm-rich impurity phase and low Fe/Ni content identified, the dark gray color is a second phase also a Fe/Ni-rich impurity phase and a low Sm content, the black color is a second phase also a Fe-rich impurity phase, and a black dot is a porosity of samples corresponding with EPMA results in Figure 4.1.3., the color mapping technique (area analysis), the stronger the red color on the color stripe, the more analytical elements will be.(3) Fe/Ni content are the same area and Ni Infiltrate the area of Fe content (white arrow and circle) and showed the distribution of Sm content. It's also rather inhomogeneities of the sample (4) which had many phases

occurred in samples. An inspection of the microphotograph of SEM-EDX and EPMA analyses indicated a component between the nominal and actual compositions of all samples in table II., the nominal and actual compositions for ST series and HP series, respectively.

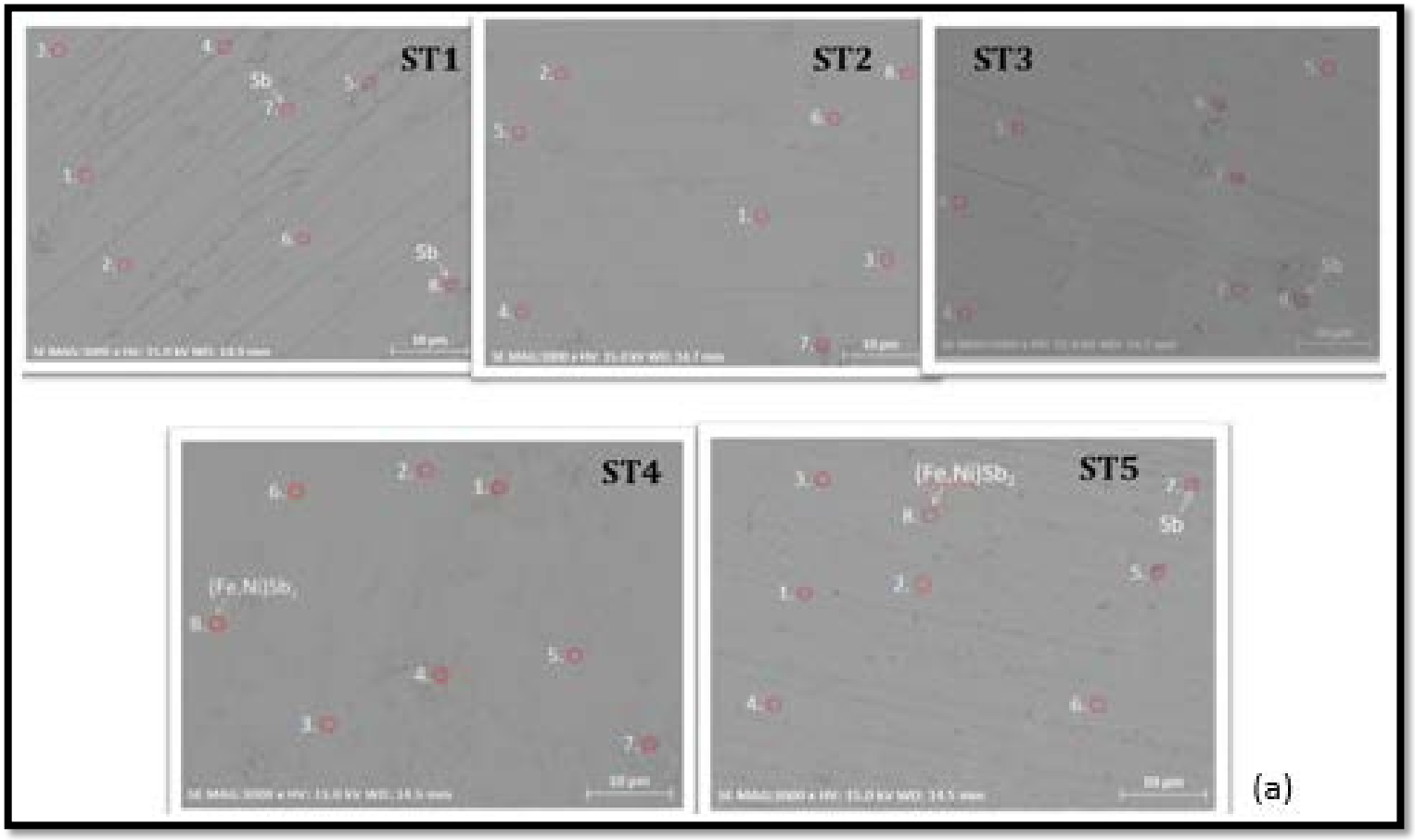

Figure. 4.1.2. SEM-EDX of $Sm_y(Fe_{1-x}Ni_x)_4Sb_{12}$ samples (a) and (b) for ST series and HP series, respectively.

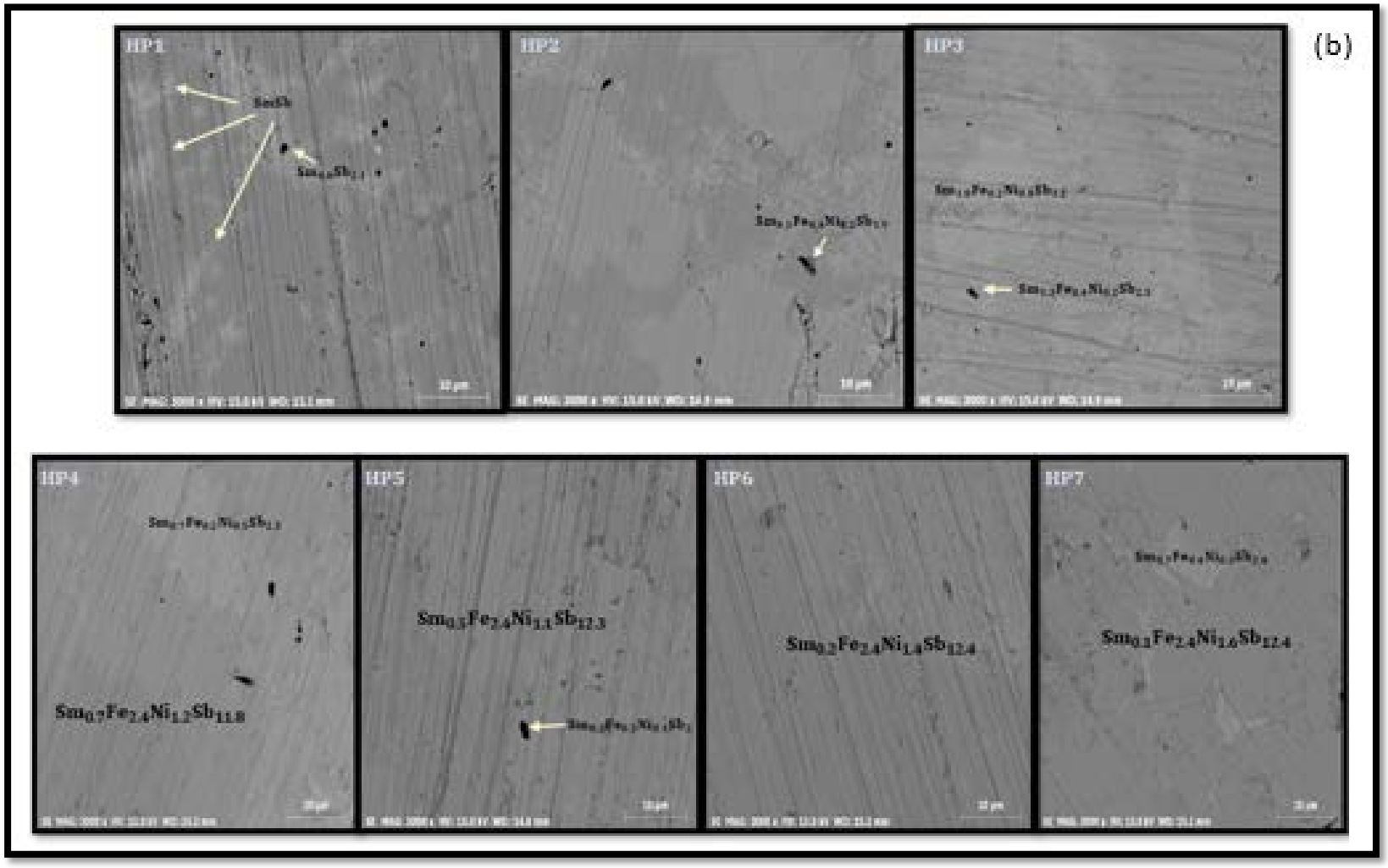

Figure. 4.1.2. SEM-EDX of $Sm_y(Fe_{1-x}Ni_x)_4Sb_{12}$ samples (a) and (b) for ST series and HP series, respectively

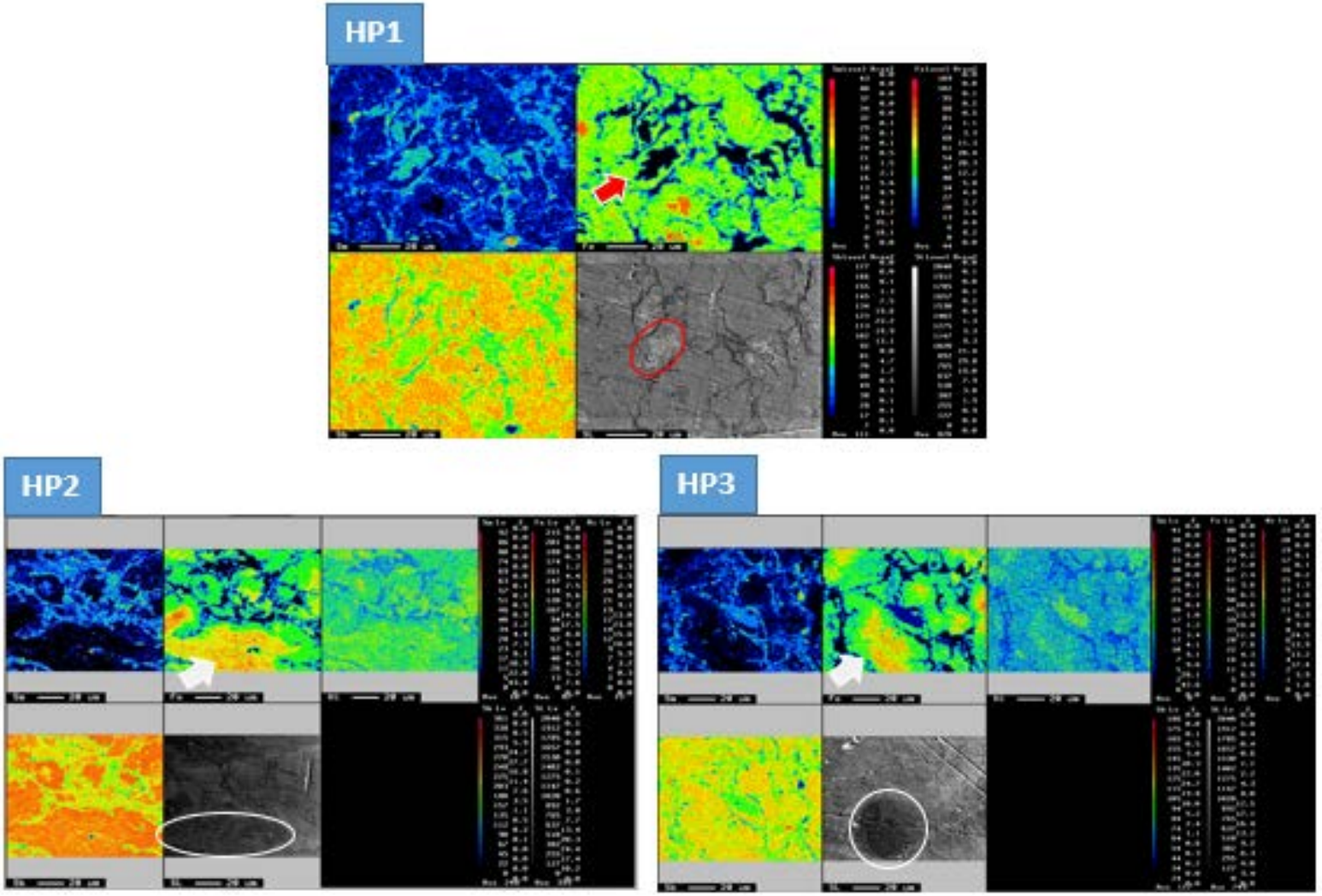

Figure. 4.1.3. EPMA of $Sm_y(Fe_{1-x}Ni_x)_4Sb_{12}$ samples for HP series.

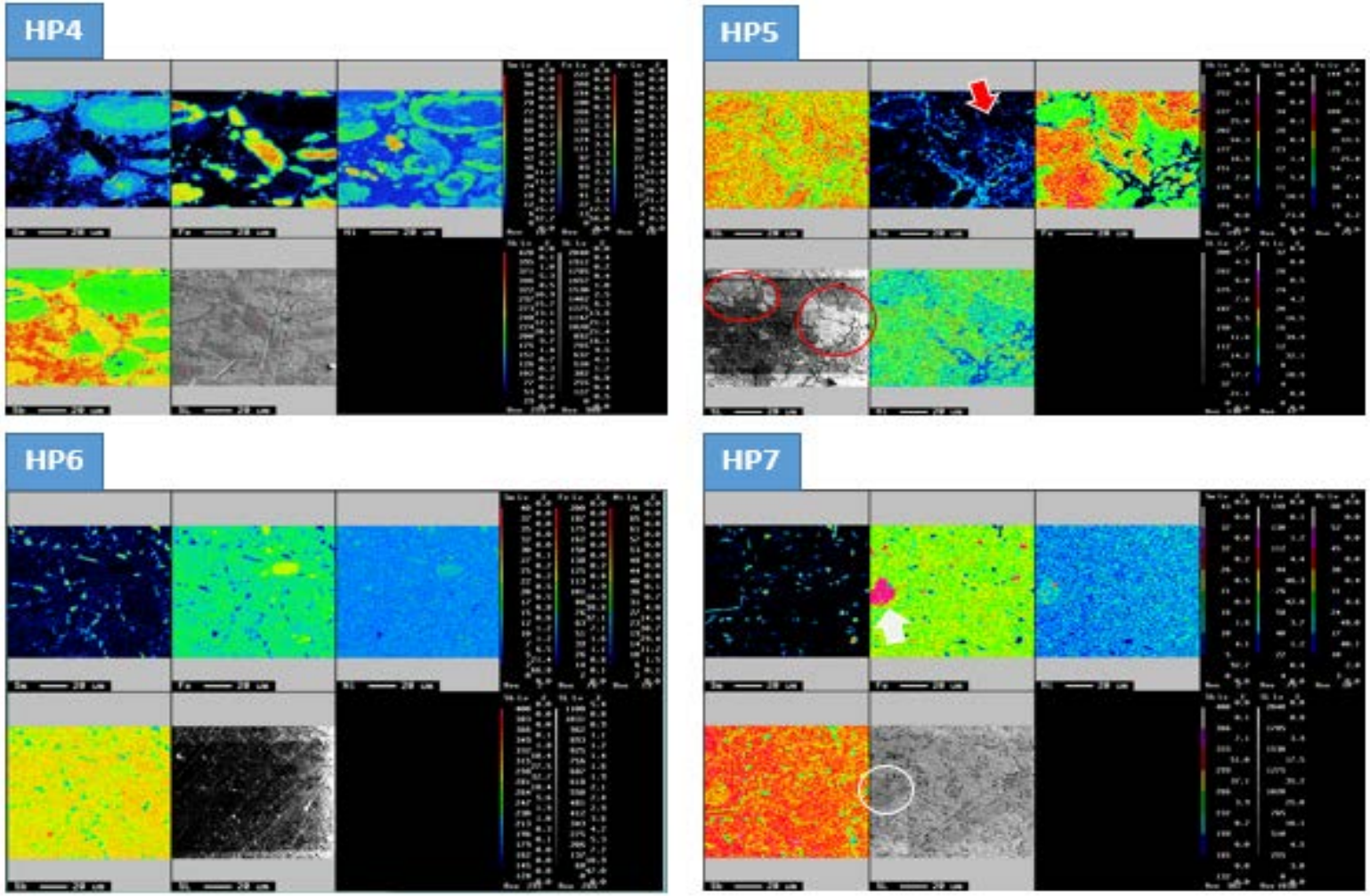

Figure. 4.1.3. EPMA of $Sm_y(Fe_{1-x}Ni_x)_4Sb_{12}$ samples for HP series.

The lattice parameters (α) for the samples were calculated by the least-squares fitting method, α and actual composition of $Sm_y(Fe_{1-x}Ni_x)_4Sb_{12}$ as shown Table. II, Filling Sm into the voids (increasing filling fraction) lead to lattice constant increase, and increasing Ni content according to the Vegard's law,(5) and Ni atomic radius smaller than Fe will lead to shrink the lattice. (6),(7) The maximum lattices constant is 9.130 Å for HP1 higher than 9.091 Å for HP7 that lowest lattice constant of 0.47%, and ST samples was 9.12(9) Å for ST1 higher than 9.09(5) Å for ST5 actual composition sample that lowest lattice constant of 0.27%, respectively.

Table II. The composition and the lattice constant of $Sm_y(Fe_{1-x}Ni_x)_4Sb_{12}$ samples.

No.	Sample	Nominal composition	Actual composition	Lattice constant (**Å**)
1.	ST1	$Sm_{0.8}Fe_{3.8}Sb_{12}$	$Sm_{0.80}Fe_4Sb_{12}$	9.130
2.	ST2	$Sm_{0.5}(Fe_{0.7}Ni_{0.2})_4Sb_{12}$	$Sm_{0.64}(Fe_{0.91}Ni_{0.09})_4Sb_{12.4}$	9.111
3.	ST3	$Sm_{0.3}(Fe_{0.6}Ni_{0.3})_4Sb_{12}$	$Sm_{0.45}(Fe_{0.73}Ni_{0.27})_4Sb_{12.6}$	9.116
4.	ST4	$Sm_{0.1}(Fe_{0.5}Ni_{0.4})_4Sb_{12}$	$Sm_{0.14}(Fe_{0.63}Ni_{0.37})_4Sb_{12.8}$	9.090
5.	ST5	$Sm_{0.04}(Fe_{0.4}Ni_{0.5})_4Sb_{12}$	$Sm_{0.04}(Fe_{0.47}Ni_{0.53})_4Sb_{11.3}$	9.095
6.	HP1	$Sm_{1.2}Fe_4Sb_{12}$	$Sm_{0.87}Fe_4Sb_{11.3}$	9.134
7.	HP2	$Sm_{1.2}(Fe_{0.6}Ni_{0.4})_4Sb_{12}$	$Sm_{0.56}(Fe_{0.54}Ni_{0.46})_4Sb_{11.2}$	9.110
8.	HP3	$Sm_{1.0}(Fe_{0.6}Ni_{0.4})_4Sb_{12}$	$Sm_{0.36}(Fe_{0.58}Ni_{0.42})_4Sb_{11.5}$	9.097
9.	HP4	$Sm_{0.8}(Fe_{0.6}Ni_{0.4})_4Sb_{12}$	$Sm_{0.22}(Fe_{0.6}Ni_{0.4})_4Sb_{12.2}$	9.092
10.	HP5	$Sm_{0.6}(Fe_{0.6}Ni_{0.4})_4Sb_{12}$	$Sm_{0.24}(Fe_{0.59}Ni_{0.41})_4Sb_{11.2}$	9.101
11.	HP6	$Sm_{0.4}(Fe_{0.6}Ni_{0.4})_4Sb_{12}$	$Sm_{0.16}(Fe_{0.63}Ni_{0.37})_4Sb_{12.8}$	9.092
12.	HP7	$Sm_{0.2}(Fe_{0.6}Ni_{0.4})_4Sb_{12}$	$Sm_{0.09}(Fe_{0.61}Ni_{0.39})_4Sb_{12.5}$	9.091

4.2. Thermoelectric properties

The temperature dependence of electrical transport properties was shown in Figure 4.2.1. (a) the electrical conductivity (σ) for $Sm_y(Fe_{1-x}Ni_x)_4Sb_{12}$ samples of HP and ST series, and (b) the electrical resistivity (ρ) of HP and ST series, respectively. Almost samples indicated a metallic-like behavior (8) due to σ values decreases successively with increasing temperature reaches room temperature, except HP2, HP3, and H5 actual composition samples indicated a semiconductor behavior(9), which probably electron-hole pairs across the energy gap from the intrinsic excitation, and the carriers being supplied by impurities acting as dopants from heavily doped semiconductors extrinsic region (7) by σ values decreases with increasing temperature at low temperature, then increases continuously with increasing temperature reach room temperature. The relation between ρ values related to σ values in the equation, $\sigma = 1/\rho$, the highest of σ of HP samples was 0.00(2) μS/cm (the lowest ρ was 585.82 μΩ.cm) of HP6 actual composition sample at room temperature.

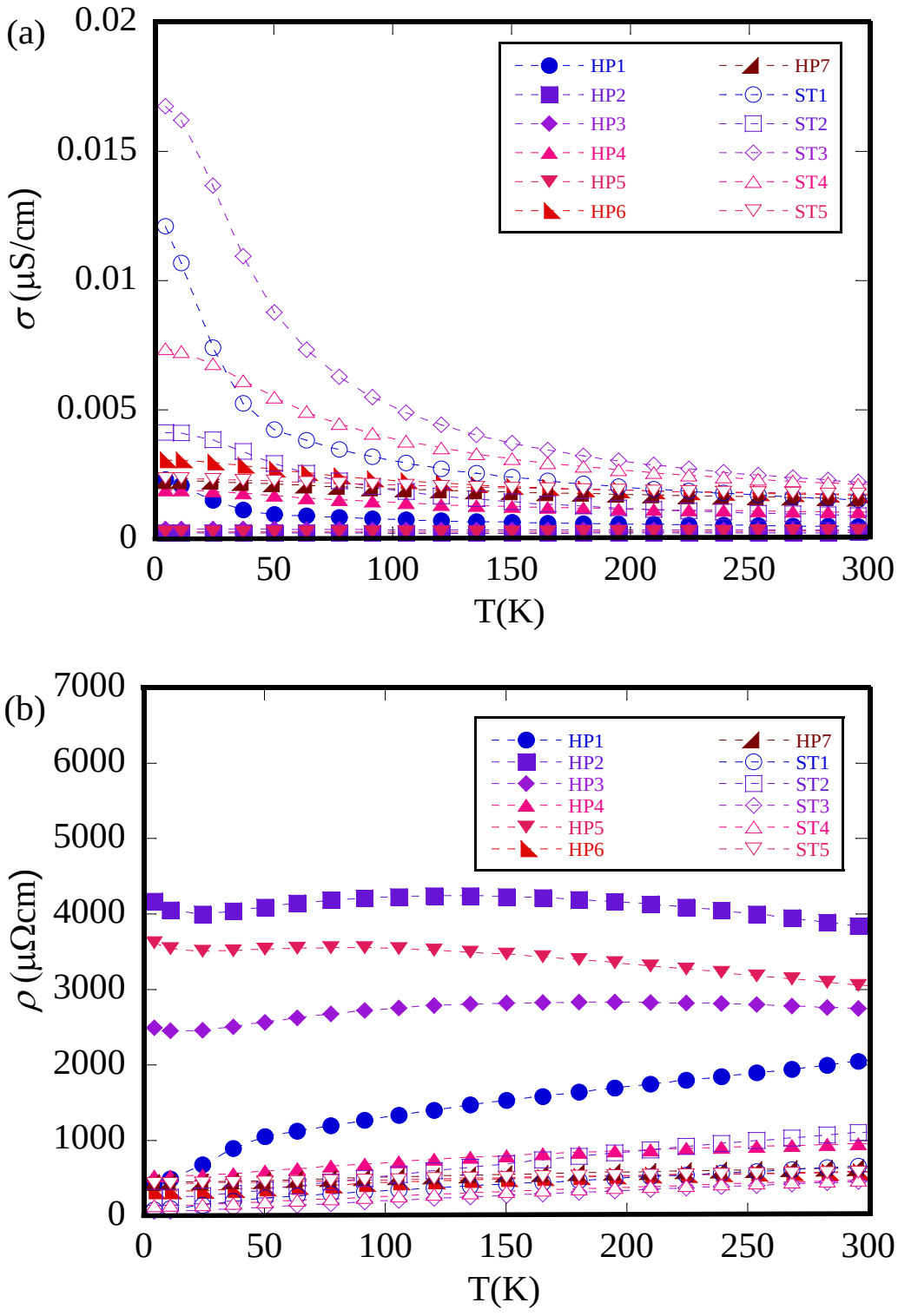

Figure 4.2.1 (a) the electrical conductivity (σ) for $Sm_y(Fe_{1-x}Ni_x)_4Sb_{12}$ samples of HP and ST series, and (b) the electrical resistivity (ρ) of HP and ST series.

The temperature dependence of Seebeck coefficient (*S*) for $Sm_y(Fe_{1-x}Ni_x)_4Sb_{12}$ samples of HP and ST series, as displayed in Figure 4.2.2., the HP1-3 and ST1-3 sample were shown the positive *S* value from the majority of charge carriers are holes. The remain HP4-7 and ST4-5 sample were shown the negative *S* value indicated most charge carriers are electrons at room temperature. The absolute value of *S* decreases from a maximum positive value was 56.66 μV/K of HP1 to a maximum negative value was -68.42 μV/K of HP7 sample at room temperature around 17.19% of absolute value. For ST samples, the absolute value of *S* decreases from a maximum positive value was 56.56 μV/K of ST2 to a maximum negative value was -47.31 μV/K of ST4 sample at room temperature around 19.55% of absolute value.

Figure 4.2.3. Shows the Seebeck coefficient (*S*) for $Sm_y(Fe_{1-x}Ni_x)_4Sb_{12}$ samples as a function of (a) Ni content, (b) Fe content, and (c) Sm content at room temperature, respectively, it can be observed that both 2 methods (HP and ST samples) displayed a high value of the *S* around p/n crossover area with Ni content around 0.2 to 0.4 corresponding with Fe content around 0.6 to 0.8, following to Vegard's law. The electrons also increased by increasing Ni-substituted for n-type skutterudites lead to the increased *S* value results. For a high value of the *S* around p/n crossover area shown a Sm-filled around 0.6 to 0.8 for HP samples and 0.1 to 0.3 for ST samples, respectively.

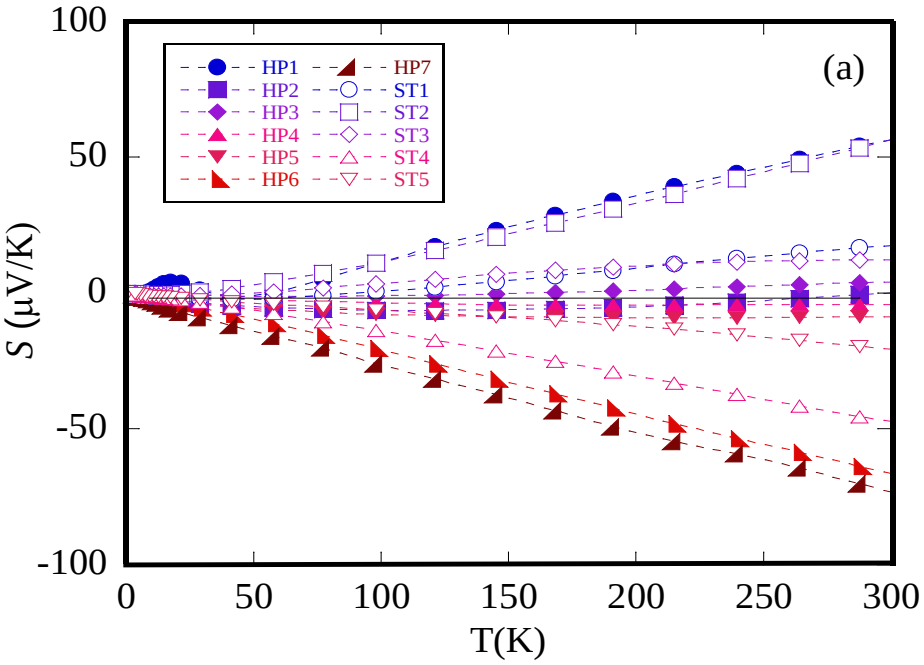

Figure 4.2.2. The temperature dependence of Seebeck coefficient (*S*) for $Sm_y(Fe_{1-x}Ni_x)_4Sb_{12}$ samples of HP and ST series.

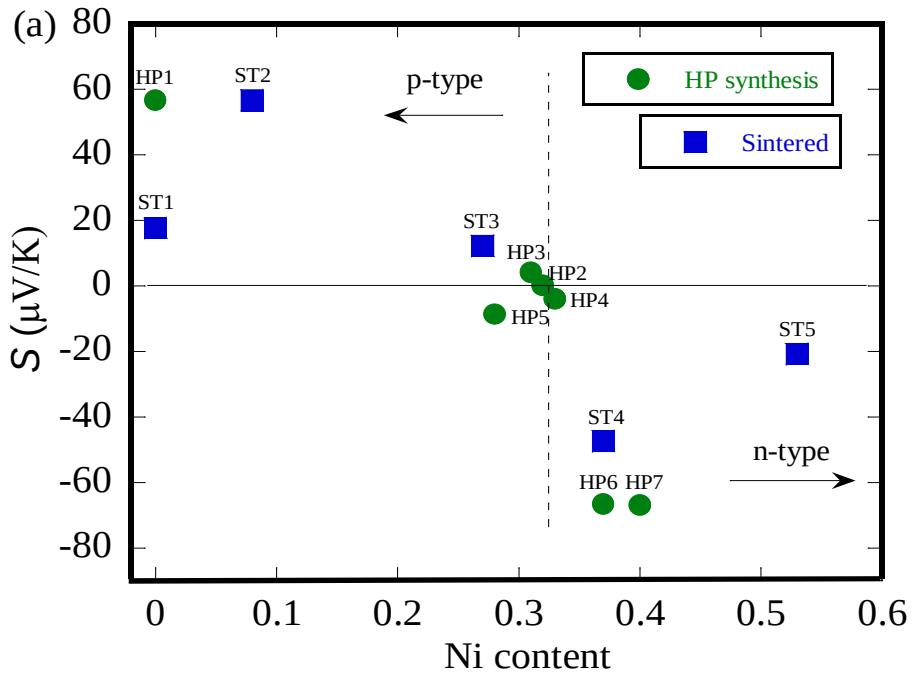

Figure 4.2.3. The Seebeck coefficient (*S*) for $Sm_y(Fe_{1-x}Ni_x)_4Sb_{12}$ samples as a function of (a) Ni content, (b) Fe content, and (c) Sm content at room temperature, respectively.

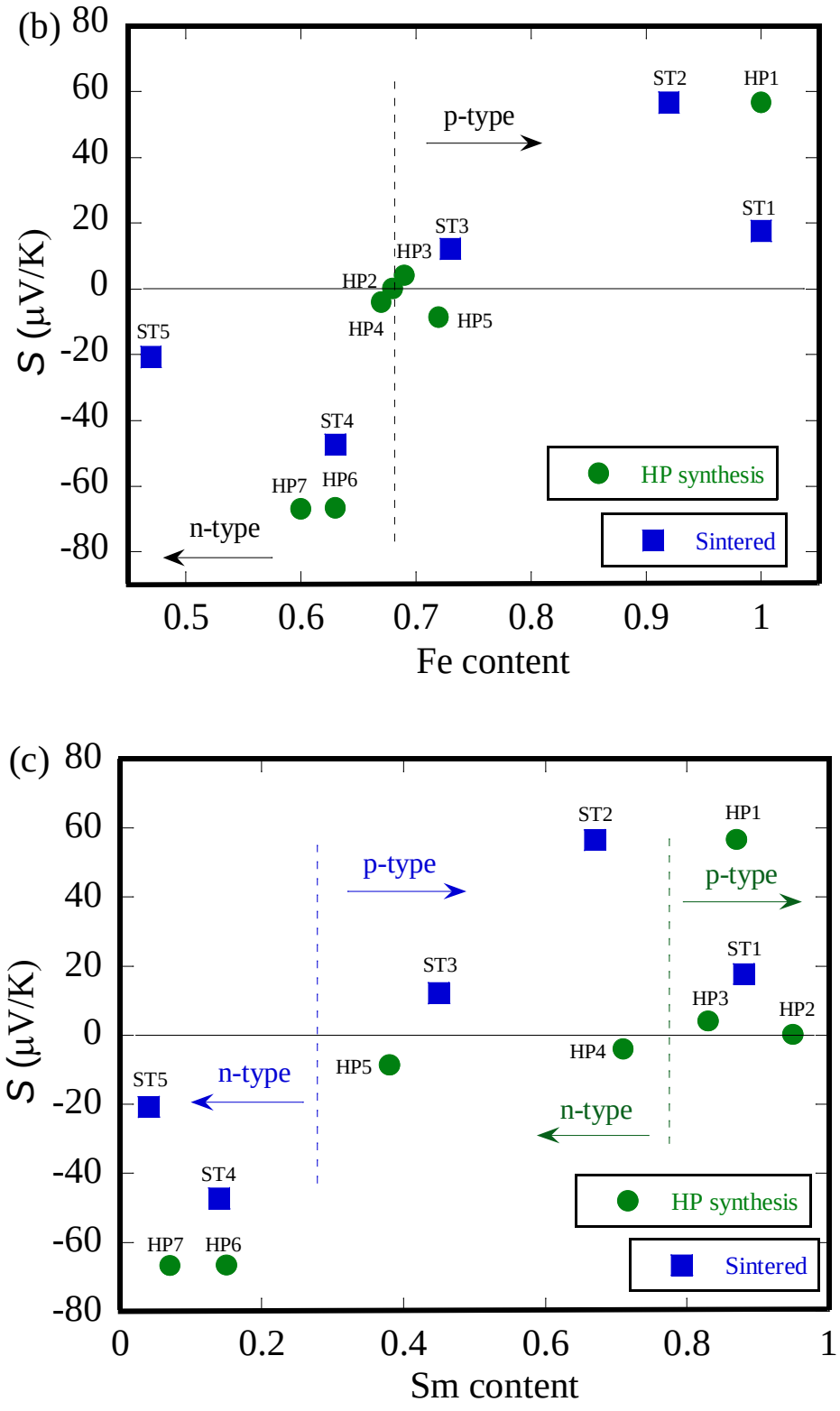

Figure 4.2.3. Shows the Seebeck coefficient (*S*) for $Sm_y(Fe_{1-x}Ni_x)_4Sb_{12}$ samples as a function of (a) Ni content, (b) Fe content, and (c) Sm content at room temperature, respectively.

The temperature dependence of thermal transport properties was shown in Figure 4.2.4. (a) the thermal conductivity (κ) of HP sample, (b) the thermal conductivity (κ) of all samples (HP and ST samples), (c) the lattice thermal conductivity (κ_L) of HP samples, and (d) the lattice thermal conductivity (κ_L) of all samples (HP and ST samples), respectively. Normally, filling fraction content addition suppresses κ values by strongly scattering thermal transport phonons, provide scattering phonon point defect and phonon resonance with a larger filling fraction in the literature data report. However, this experiment results, the effects of κ values also depended on Ni/Fe content further reduce κ_E values following the Wiedmann-Franz law, the lowering electronic contribution of κ values because of degradation in σ values, increase Ni content quite corresponding with increasing σ values, and the dominant scattering mechanism is impurity scattering (7) in the low-temperature range as well. Figure 4.2.4. (d) displays the lowest κ_L value of all series (0.16 W/mK) decrease from κ value (1.31 W/mK) was 87.78 % of HP7 indicated Umklapp phonon-phonon scattering(6),(7) by increase κ_L values at low temperature and then decrease reach room temperature due to the bipolar diffusion.(10),(11)

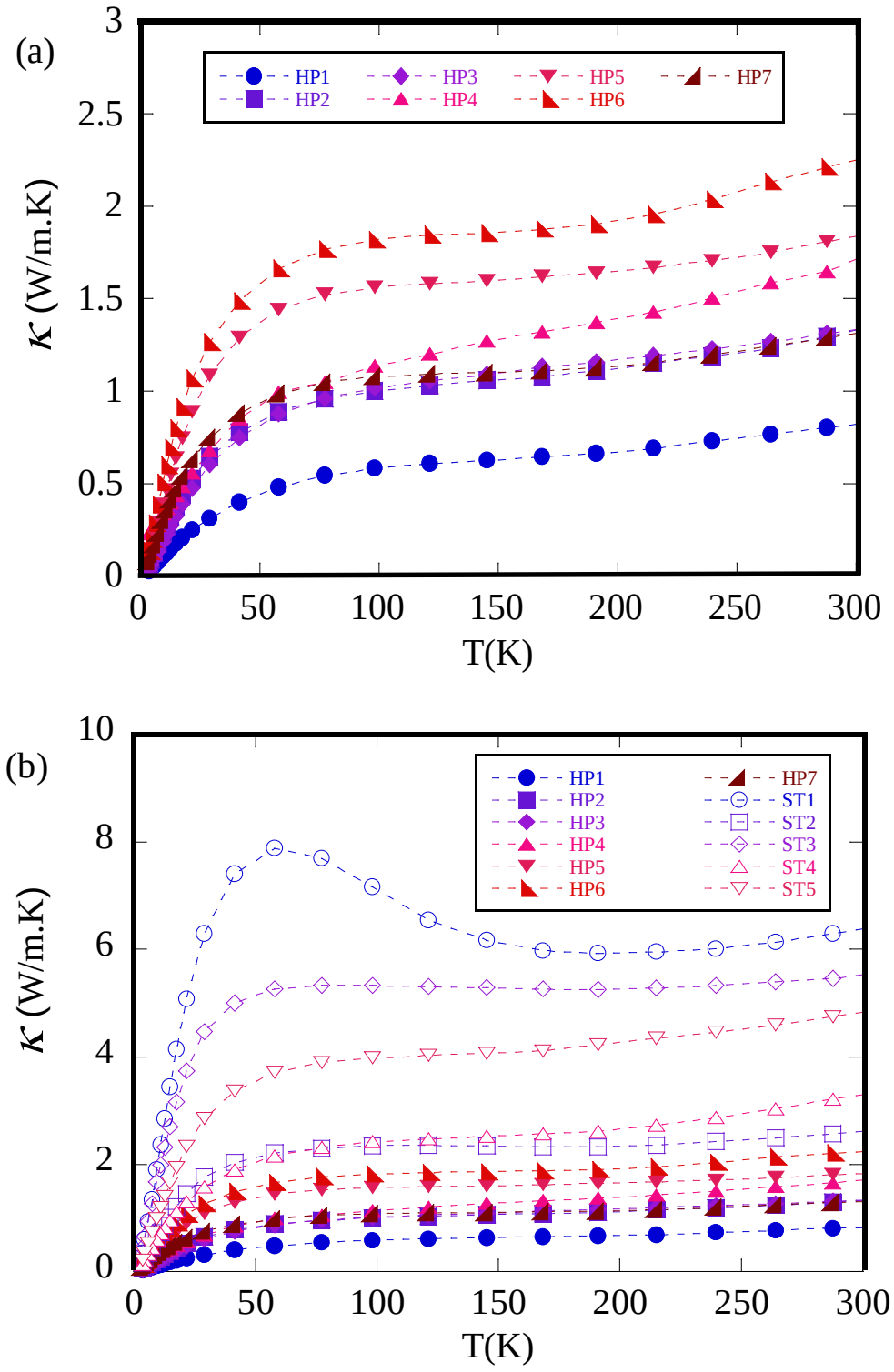

Figure 4.2.4. (a) (b) The temperature dependence of the thermal conductivity (κ) of $Sm_y(Fe_{1-x}Ni_x)_4Sb_{12}$.

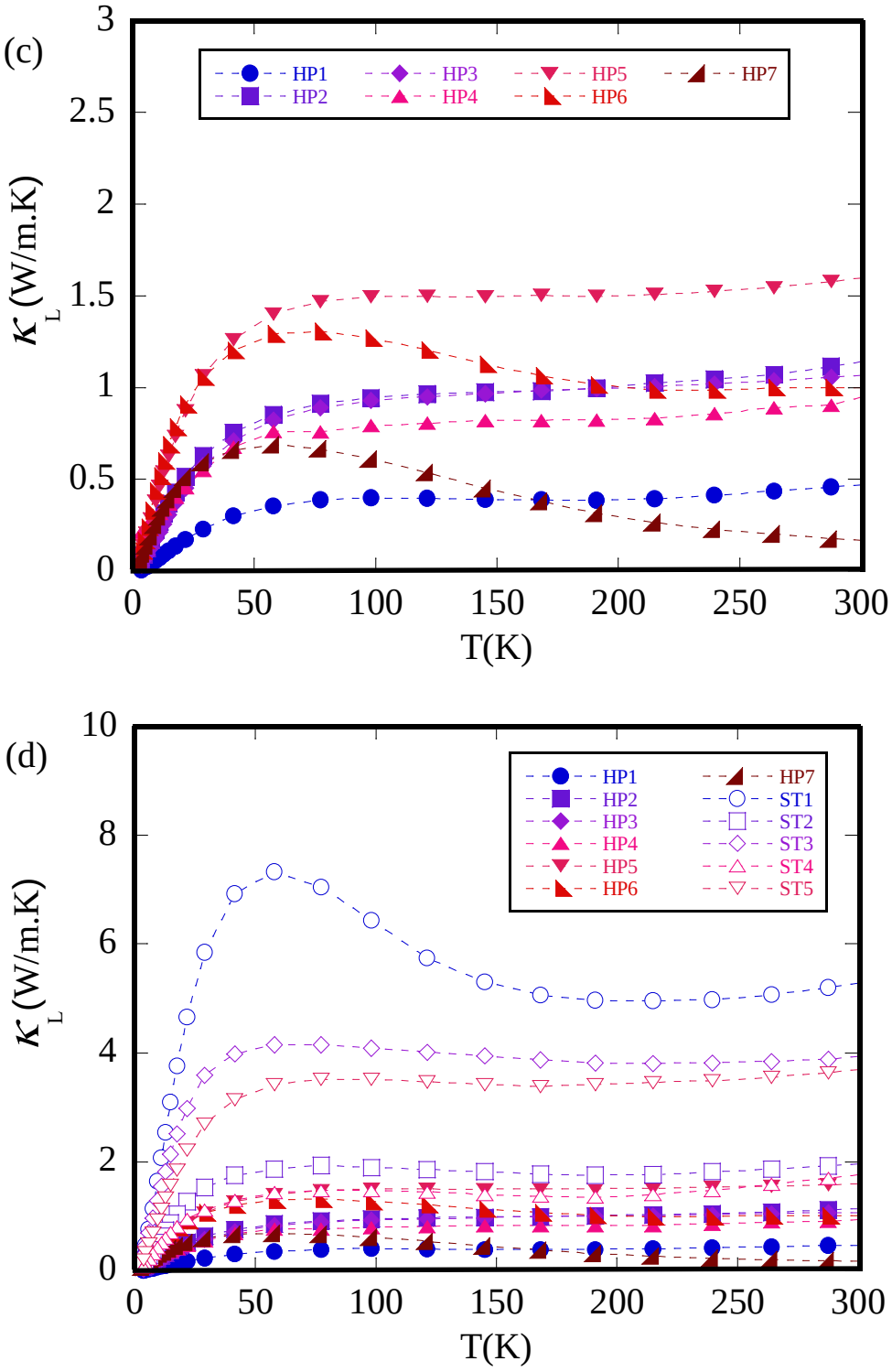

Figure 4.2.4. (c), (d) The temperature dependence of the lattice thermal conductivity (κ_L) of $Sm_y(Fe_{1-x}Ni_x)_4Sb_{12}$.

The mobility concentration (μ_H) was calculated by using the equation $\mu_H = 1/\rho R_H$, where ρ is the electrical resistivity, and R_H is the Hall coefficient, the carrier concentration (n) was calculated from R_H by using the equation $n = 1/(eR_H)$, which e is the elementary charge. The symbol of R_H indicated that the major of carrier changed, the negative are electrons (n-type) and the positive are holes (p-type).(7),(3) The n should continuously decrease with increasing Ni content due to a compensate for the electron in compounds, as shown n and μ_H values in Table III., the results of these experiments show the ZT values increase with increasing temperature reaches room temperature.

Figure 4.2.5. (a) displays the temperature dependence of the carrier concentration (n), the n values are on the order between 10^{19}-10^{20} cm^{-3}, indicated a semiconductor behavior. Figure 4.2.5. (b) displays the mobility concentration (μ_H) of $Sm_y(Fe_{1-x}Ni_x)_4Sb_{12}$ samples at room temperature, the trend of $\mu_H \alpha T^{-3/2}$ behavior indicated that the acoustic phonon scattering (12) dominates at above 100 K, which corresponding with thermal transport properties as shown in Figure 5. (b), the κ_L of $Sm_y(Fe_{1-x}Ni_x)_4Sb_{12}$ samples at room temperature.

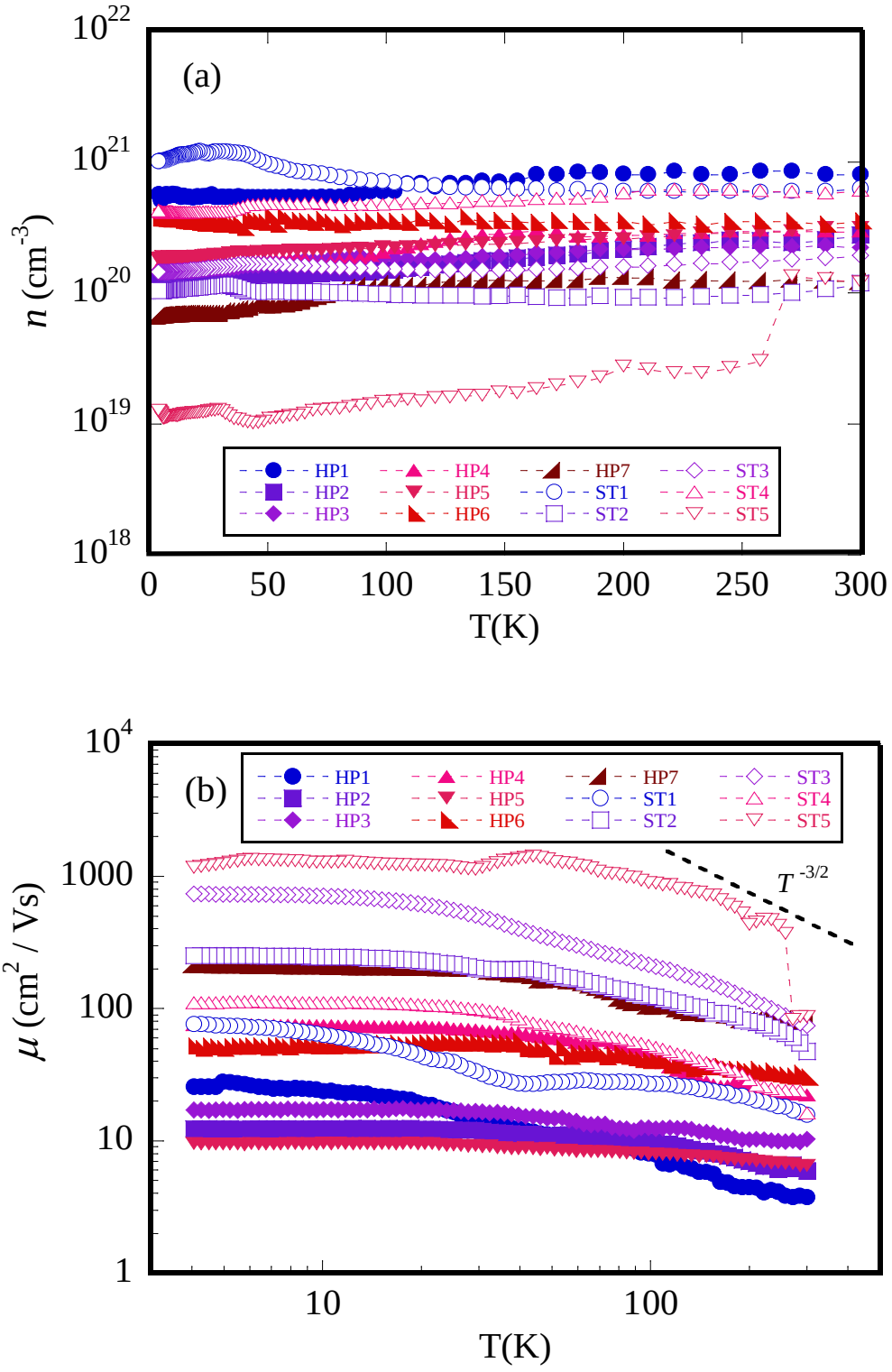

Figure 4.2.5. (a) The temperature dependence of the carrier concentration (n) and (b) The mobility concentration (μ_H) of $Sm_y(Fe_{1-x}Ni_x)_4Sb_{12}$ samples at room temperature.

As the measured thermal and electrical transport properties, the dimensionless Figure of merit (*ZT*) value has been calculated in Figure 4.2.6. *ZT* values as a function of the temperature of $Sm_y(Fe_{1-x}Ni_x)_4Sb_{12}$ samples, and the TE properties of $Sm_y(Fe_{1-x}Ni_x)_4Sb_{12}$ samples at room-temperature are tabulated in Table III., respectively. The results of these experiments show the *ZT* values increase with increasing temperature reaches room temperature, the highest *ZT* values of 0.167(7) was achieved of HP7 sample, which is interestingly higher than the unfilled skutterudites HP1 sample of 0.056(1) around 66.55 % at room temperature, according to the result of the high *S* and the low κ interestingly were reduced by scattering of phonons. Based on these results, the maximum *ZT* values adjusted by tuning Sm-filled and Fe/Ni content of these skutterudites compounds, increasing Ni content and decreasing Sm-filled moves the maximum *ZT* values possible to change this material according to the desired temperature range.

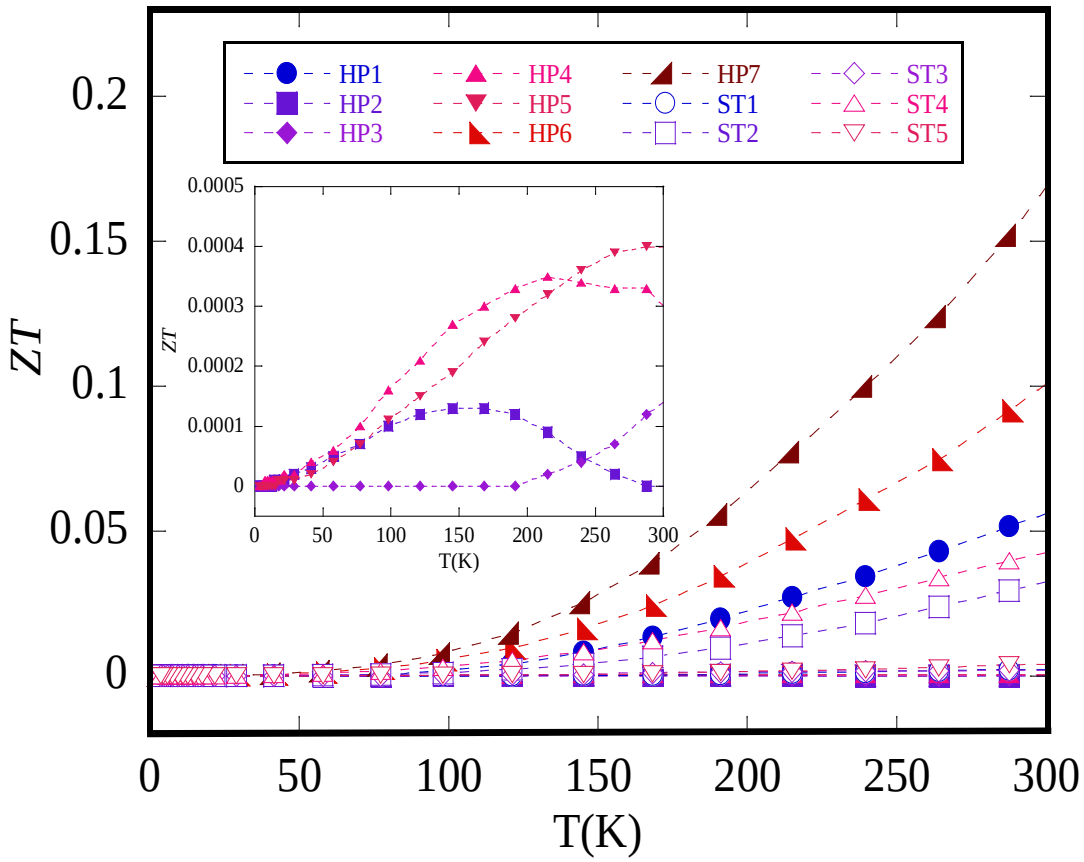

Figure 4.2.6. *ZT* values as a function of the temperature of $Sm_y(Fe_{1-x}Ni_x)_4Sb_{12}$ samples.

.

Table III. The TE properties of $Sm_y(Fe_{1-x}Ni_x)_4Sb_{12}$ samples at room temperature.

No.	Actual composition	ρ (mΩ)	σ (S/m)	κ (W/mK)	κ_L (W/mK)	S (V/K)	Type	n ($10^{20}cm^{-3}$)	μ_H (cm^2/Vs)	ZT
1. HP1	$Sm_{0.87}Fe_4Sb_{11.3}$	2.07E-05	4.83E+04	0.83	0.47	5.66E-05	P	8.10	3.74	0.056(1)
2. HP2	$Sm_{0.56}(Fe_{0.54}Ni_{0.46})_4Sb_{11.2}$	3.82E-05	2.62E+04	1.34	1.14	1.23E-07	P	2.77	5.90	8.89E-08
3. HP3	$Sm_{0.36}(Fe_{0.58}Ni_{0.42})_4Sb_{11.5}$	2.74E-05	3.65E+04	1.34	1.07	4.14E-06	P	2.22	10.29	0.000(1)
4. HP4	$Sm_{0.22}(Fe_{0.6}Ni_{0.4})_4Sb_{12.2}$	9.65E-06	1.04E+05	1.72	0.95	-4.06E-06	N	2.95	22.20	0.000(3)
5. HP5	$Sm_{0.24}(Fe_{0.59}Ni_{0.41})_4Sb_{11.2}$	3.04E-05	3.29E+04	1.84	1.60	-8.67E-06	N	3.16	6.51	0.000(4)
6. HP6	$Sm_{0.16}(Fe_{0.63}Ni_{0.37})_4Sb_{12.8}$	5.86E-06	1.71E+05	2.25	1.00	-6.66E-05	N	3.53	30.21	0.100(9)
7. HP7	$Sm_{0.09}(Fe_{0.61}Ni_{0.39})_4Sb_{12.5}$	6.38E-06	1.57E+05	1.31	0.16	-6.84E-05	N	1.21	81.17	0.167(7)
8. ST1	$Sm_{0.80}Fe_4Sb_{12}$	6.63E-06	1.51E+05	6.38	5.28	1.77E-05	P	6.22	15.61	0.002(2)
9. ST2	$Sm_{0.6}4(Fe_{0.91}Ni_{0.09})_4Sb_{12.4}$	1.12E-05	8.93E+04	2.62	1.96	5.66E-05	P	1.18	47.43	0.032(7)
10.ST3	$Sm_{0.45}(Fe_{0.73}Ni_{0.27})_4Sb_{12.6}$	4.55E-06	2.20E+05	5.52	3.92	1.22E-05	P	1.91	73.82	0.001(7)
11.ST4	$Sm_{0.14}(Fe_{0.63}Ni_{0.37})_4Sb_{12.8}$	4.76E-06	2.10E+05	3.29	1.76	-4.73E-05	N	6.02	16.28	0.042(7)
12.ST5	$Sm_{0.04}(Fe_{0.47}Ni_{0.53})_4Sb_{11.3}$	6.37E-06	1.57E+05	4.83	3.69	-2.08E-05	N	1.20	86.95	0.004(2)

4.3 Summary

The skutterudite compounds $Sm_y(Fe_{1-x}Ni_x)_4Sb_{12}$ were successfully synthesized by the high-pressure synthesis (HPS) technique. The HPS can also modify, i.e. grain size, texture, morphology, defect structure, and concentration (13),(4) by varying the pressure and temperature conditions to improve TE properties. The TE properties concluded the results as follows, X-ray diffraction, SEM, EDX, and EPMA results were showed skutterudite main phase, and the lattice constants were changed from the increase of Ni content as the result of shrinking the lattice constant values. In addition, the increase of Sm-filled leads to the increase of lattice constant value as well. The Sm-filled and Ni-substitution effects on the TE properties of $Sm_y(Fe_{1-x}Ni_x)_4Sb_{12}$ series were studied by the results of both electrical and thermal transport properties. The increase Ni content quite corresponding with increasing σ values, also shows the low κ_L value indicated Umklapp phonon-phonon scattering by increase κ_L at low temperature and continuous decreases reach room-temperature, respectively. Furthermore, tuning Sm-filled and Fe/Ni content could be established the p-type and n-type skutterudite. The high of S values shown around p/n crossover area with Ni content around 0.3 corresponding with Fe content around 0.7 consist the n and μ_H confirmed by Hall effect measurement. The highest ZT value of 0.167(7) is achieved for $Sm_{0.09}(Fe_{0.61}Ni_{0.39})_4Sb_{12.5}$ (HP7) actual composition of n-type skutterudite at room temperature.

4.4 References

1. Sekine C, Mori Y. Development of thermoelectric materials using high-pressure synthesis technique. Jpn J Appl Phys. 2017;56(5):0–6.

2. Mi JL, Zhao XB, Zhu TJ, Tu JP, Cao GS. Solvothermal synthesis of nanostructured ternary skutterudite $Fe_{0.5}Ni_{0.5}Sb_3$. J Alloys Compd. 2005;399(1–2):260–3.

3. Rowe EDM, Ph D, Sc D, Group F. HANDBOOK. 2006. 72-82.

4. Taylor P. High Pressure Research : An High-pressure synthesized materials : treasures and hints. 2007;(June 2012):37–41.

5. Rogl G, Grytsiv A, Royanian E, Heinrich P, Bauer E, Rogl P. New p- and n-type skutterudites with ZT > 1 and nearly identical thermal expansion and mechanical properties. Acta Mater. 2013;61(11):4066–79.

6. Tan G, Zheng Y, Yan Y, Tang X. Preparation and thermoelectric properties of p-type filled skutterudites $Ce_yFe_{4-x}Ni_xSb_{12}$. J Alloys Compd. 2014; 584:216–21.

7. Nolas GS, Morelli DT, Tritt TM. Skutterudites: a phonon-glass-electron crystal approach to advanced thermoelectric energy conversion applications. Annu Rev Mater Sci. 1999;29:89–116.

8. Zhao XY, Shi X, Chen LD, Zhang WQ, Zhang WB, Pel YZ. Synthesis and thermoelectric properties of Sr-filled skutterudite Sr yCo4Sb12. J Appl Phys. 2006;99(5).

9. Artini C, Castellero A, Baricco M, Buscaglia M T and Carlini R, J. Solid State Sci. 2018;79:71-78.

10. Choi S, Kurosaki K, Ohishi Y, Muta H, Yamanaka S. Thermoelectric properties of Tl-filled Co-free p-type skutterudites: $Tl_x(Fe,Ni)_4Sb_{12}$. J Appl Phys. 2014;115(2).

11. Zhang J, Xu B, Yu F, Yu D, Liu Z, He J, et al. Thermoelectric properties of n-type $CoSb_3$ fabricated with high pressure sintering. 2010;503:490–3.

12. Alboni PN, Ji X, He J, Gothard N, Tritt TM, Alboni PN, et al. nanocomposites. 2008;113707(May 2013):3–8.

13. Drahansky M, Paridah M., Moradbak A, Mohamed A., Owolabi F abdulwahab taiwo, Asniza M, et al. We are IntechOpen, Intech. 2016;

Chapter 5 Conclusion

5.1 Conclusion

Nowadays, there is a growing interest in the use of renewable energy. To harvest natural energy from the environment to provide sustainable, green, and inexpensive electrical energy such as RF, heat radiation, solar energy, vibration / mechanical energy, and others, as well as convert heat into electrical energy to produce electronic devices and industrial machinery is expanding exponentially. (1) Heat energy is one of the energy sources from many places. That can be found in many sectors, in electronic operations, devices (integrated circuits, telephones, computers, etc.) are working, vehicles, in the building sector, and even in the human body.

Thermoelectric generators (TEGs) are active devices consisting of converting heat energy into electrical energy.(1) TEGs are made of dissimilar thermocouples, based on the Seebeck effect, connected electrically in series and thermally in parallel. TEGs are widely used in many fields due to interesting features such as energy-saving, free maintenance, and long-life span. They become an interesting area in the field of energy harvesting for large and small applications depending on the size of delivery power and materials used.

The potential of thermoelectric (TE) is evaluated by the dimensionless figure of merit (ZT), $ZT=S^2\sigma T/\kappa$,[1,2] where S is the Seebeck coefficient, T is the absolute temperature, σ is the electrical conductivity, and κ is the thermal conductivity, respectively. Moreover, κ is constituted by an electronic thermal conductivity (κ_E), directly related to σ followed by the Wiedemann-Franz law(2), (3) $\kappa_E=\sigma L_0 T$, where L_0 is the Lorentz constant (2.44×10^{-8} $W\Omega/K^2$), and κ_L is a lattice thermal conductivity.

Filled skutterudite compounds are one type of TE that suitable for the use of advanced TE potentials of applications. It has been studied as one of the most

promising TE based on state-of-the-art TE materials possess the feature of Phonon Glass Electron Crystal (PGEC) concept(4),(5) implying, these have a phonon of crystal that is “glass-like” behavior, lattice thermal conductivity like amorphous material but an electronic structure like solid crystalline. The formula was RT_4X_{12}, where *R* is guest atom such as alkali metal, alkaline earth, lanthanide, and actinide, *T* is transition metals such as Fe, Ru, Os, Pt, and *X* is non-metals such as P, As, Sb, Ge, respectively. The random motion (rattling) (4),(6) of *R* inside the X_{12} voids to scatter the phonon in the crystal structure, which responsible for a substantial decrease in κ_L to affects the electrical transport properties and enhance the figure of merit *ZT* values. The devaluation efforts of κ_L could cause a decrease of κ without reducing *PFs*, aggregated excellent TE will result in high *ZT* values by high *S* combined with high σ and low κ values.

Literature has been reported Sm fillers atoms get the attention of donating electrons to the crystals had improved *PFs* and κ_L value by rattling effect. The maximum *ZT* value of 0.55 has been achieved for p-type of the $Sm_y(Fe_{1-x}Ni_x)_4Sb_{12}$ skutterudites compound prepared by melting, quenching and annealing.(7) These substance has never been prepared by using high-pressure synthesis (HPS) technique before, which this method helps to usually take a few hours, estimated a decrease in synthetic temperature and the densification rate can be improved by a pressure, such as the relaxation of the n-type defects, a reduction in grain size (6), (8) to reduce κ values, power factor (*PFs*) resulting in improved TE properties the concentration of high the Sm-filled, also obtaining material properties more rapidly, and cleanly than the other chemical techniques.

The potential *ZT* should be achieved by carefully expanding the areas of synthesis with the tune the Sm filling ratio, also the Fe/Ni substitution around the p/n crossover area is attributed to the increase of *S* values.(9) The TE properties can be tuned by the Sm-filled and the substitution Fe/Ni content, the p/n crossover of $Sm_y(Fe_{1-x}Ni_x)_4Sb_{12}$ at Fe $\approx$ 0.63, and Sm $\approx$ 0.31 confirmed by measurements of *S* values prepared by direct reaction of the elements at room-temperature(10),

also at Fe ≈ 0.60, and Sm ≈ 0.33 confirmed by measurements of *S* values prepared by spark plasma sintering (SPS).(11) In this study, investigated the TE properties of p-type and n-type filled skutterudites $Sm_y(Fe_{1-x}Ni_x)_4Sb_{12}$ prepared by HPS technique, TE properties data are evaluated, including in-depth about the potential of TE, **$Sm_y(Fe_{1-x}Ni_x)_4Sb_{12}$** was successfully in synthesized under high pressure, HPS using multi-anvil press made it possible to enlarge the variation of TE material design. The highest ZT value of **0.167** was achieved for n-type skutterudite (HP7) at room temperature.

5.1 References

1. Jaziri N, Boughamoura A, Müller J, Mezghani B, Tounsi F, Ismail M. A comprehensive review of Thermoelectric Generators: Technologies and common applications. Energy Reports. 2019;
2. Rogl G, Grytsiv A, Royanian E, Heinrich P, Bauer E, Rogl P. New p- and n-type skutterudites with ZT > 1 and nearly identical thermal expansion and mechanical properties. Acta Mater. 2013;61(11):4066–79.
3. Zhang J, Xu B, Yu F, Yu D, Liu Z, He J, et al. Thermoelectric properties of n-type $CoSb_3$ fabricated with high pressure sintering. 2010;503:490–3.
4. Rowe EDM, Ph D, Sc D, Group F. HANDBOOK. 2006.
5. Nolas GS, Morelli DT, Tritt TM. Skutterudites: a phonon-glass-electron crystal approach to advanced thermoelectric energy conversion applications. Annu Rev Mater Sci. 1999;29:89–116.
6. Drahansky M, Paridah M., Moradbak A, Mohamed A., Owolabi F abdulwahab taiwo, Asniza M, et al. We are IntechOpen, Intech. 2016.
7. Carlini R, A. U. Khan, Ricciardi R, Mori T and Zanicchi G, J. Alloys Compd. 2016;655:321-326.

8. Taylor P. High Pressure Research : An High-pressure synthesized materials : treasures and hints. 2007;(June 2012):37–41.

9. Becker A, Schierning G, Theissmann R, Meseth M, Benson N, Schmechel R, et al. A sintered nanoparticle p-n junction observed by a Seebeck microscan. J Appl Phys. 2012;111(5).

10. Cristina A, Zanicchi G, Costa G A, Carnasciali M M, Fanciulli C, and Carlini R. Inorg. Chem. 2016; 55:2574-2583.

11. Artini C, Latronico G, Carlini R, Saini S, Takeuchi T, Choi S, et al. ES Materials & Manufacturing. 2019;12:29–37.

Appendix A

Journals

1. Phuangyod A, Hayashi J, Kawamura Y, Artini C, Latronico G, Carlini R, et al. Low temperature thermoelectric properties of p-type and n-type filled skutterudite compounds $Sm_y(Fe_{1-x}Ni_x)_4Sb_{12}$ prepared under high pressure. Jpn J Appl Phys. 2020; 061004.

2. Sekine C, Osanai T, Ponmani H, Phuangyod A, Kawamura Y, Gotou H. High temperature and high-pressure synthesis and magnetic properties of arsenic-based filled skutterudite compounds. Solid State Phenom. 2019;289 SSP: 85–92.

Conference

1. Phuangyod A, Artini C, Latronico G, Carlini R, Mele P, Kawamura Y, Sekine C. (2019). High-pressure synthesis of filled skutterudite compounds $Sm_y(Fe_{1-x}Ni_x)_4Sb_{12}$, 60th High Pressure Conference, Japan High Pressure Society, Sapporo, Japan, October 23, 2019.

2. Tippayamalee P, Phuangyod A, Mele P, Kawamura Y, Sekine C. (2019). High-pressure synthesis and physical properties of $R_2Pd_3Ge_5$ (R=Nd and Yb), 60th High Pressure Conference, Japan High Pressure Society, Sapporo, Japan, October 23, 2019.

3. Phuangyod A, Kawamura Y, Artini C, Latronico G, Carlini R, Saini S, Mele P, Sekine C. (2019), Thermoelectric properties of filled skutterudite compounds $Sm_y(Fe_{1-x}Ni_x)_4Sb_{12}$ using high-pressure synthesis technique, ICT2019 - 38^{th} International Conference on Thermoelectrics, Gyeongju, South Korea, June 30, 2019.

4. Phuangyod A, Sirimart J, Mona Y, Kawamura Y, Artini C, Latronico G, Mele P, Sekine C. (2019). Thermoelectric properties of filled skutterudite compounds $Sm_y(Fe_{1-x}Ni_x)_4Sb_{12}$ prepared under high pressure, the Joint Seminar on Environmental Science and Disaster Mitigation Research 2019, Muroran, Japan, March 1, 2019.

5. Phuangyod A, Sirimart J, Mona Y, Kawamura Y, Sekine C, Artini C, Latronico G, Mele P. (2018). The transport properties of filled skutterudite compounds $Sm_y(Fe_{1-x}Ni_x)_4Sb_{12}$, Muroran-IT Rare Earth Workshop 2018 , Muroran Institute of Technology, Research Center for Environmentally Friendly Materials Engineering, HaRP, Toya, Hokkaido, Japan, November 8, 2018.

6. Phuangyod A, Sirimart J, Mona Y, Kawamura Y, Sekine C, Artini C, Latronico G, Mele P. (2018). Thermoelectric properties of filled skutterudite compounds $Sm_y(Fe_{1-x}Ni_x)_4Sb_{12}$, 2018 Conference on Electrical and Information Related Society Hokkaido Branch, Proceedings of 2018 Conference on Electrical and Information Related Society Hokkaido Branch, Sapporo, Japan, October 27, 2018.

Society member

1. International Thermoelectric Society (ITS)